Investigation of the Heat Transfer Mechanism on the Performance of Polystyrene Foam Insulation

Investigation of the Heat Transfer Mechanism on the Performance of Polystyrene Foam Insulation

:   **Student : Pen-Chang Tseng**

:   **Advisor: Chiun-Hsun Chen**

                                       Hsin-Sen Chu

A Thesis

Submitted to Department of Mechanical Engineering

National Chiao Tung University

in partial Fulfillment of the Requirements

for the Degree of

Doctor of Philosophy

in

Mechanical Engineering

April 2010

Hsinchu, Taiwan, Republic of China

PE　　　　　PS

42　　　　　　　　　　　　　　　　　　　　PE

2%　PE　　　　　　　　　　　　　　　　　　　　　　PE

5%

4. 4($mWm^{-1}K^{-1}$)

80%

Investigation of the Heat Transfer Mechanism on the Performance of Polystyrene Foam Insulation

Student   Pen-Chang Tseng   Advisor   Chiun-Hsun Chen
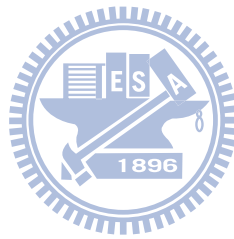
                                                       Hsin-Sen Chu

Abstract

The effects of adding Polythene (PE) in (polystyrene) PS foaming material on the cell structure and the heat transfer of vacuum insulation panels (VIPs) are examined in this study. Totally 42 samples were fabricated and analyzed to examine the influence of porous foam structure and PE additive on VIP performance. The samples were produced by in-house equipment that was able to vary the foam structure by modulating the process temperature and pressure. Several parameters were proposed to describe the foam structure, namely, the broken cell ratio, the average cell size and the solid volume fraction. Under a specific solid volume fraction, the average cell size and the broken cell ratio are linearly correlated, and it was found that an optimum cell size exists such that the total heat transport is minimal. Furthermore, these parameters are also suitable for characterizing heat transfer coefficients of thermal radiation and other heat transports. Adding 2% PE was effective in altering the cell structure and reducing the heat transfer, while adding 5% PE did not improve the performance further. The lowest thermal conductivity found in this study is 4.4 $mWm^{-1}K^{-1}$, which is among the best published performances of VIP. The magnitude of solid conduction is mainly decided by the solid volume fraction and accounts for more than 80% of the total heat

transport in VIPs. The rule of thumb of reducing VIPs' heat transport is to decrease the solid volume fraction as much as possible, while maintaining an optimal average cell size. Nevertheless, attention should be paid to balancing solid conduction and thermal radiation. The reduction of solid volume fraction is normally accompanied by the decrease of solid mass, leading to weaker structural support such that smaller cell size is required to maintain structure integrity. The decrease of solid mass is therefore accompanied by slimmer struts and thinner membrane, which may largely enhance thermal radiation.

TABLE OF CONTENTS

LIST OF TABLES

LIST OF FIGURES

NOMENCLATURE

d_c — cell size (μm)

e_b — the emitted blackbody energy flux, (W/m^2)

$e_{\lambda b}$ — Planck's spectral distribution of emissive power, ($W/(m^2 \cdot \mu m)$)

f_s — solid volume fraction, V_s/V_t, eq.(15)

f_{s+g} — volume fraction of combined solid and gas, ($V_{ub} + V_s)/V_t$.

i_λ — spectral intensity of radiant energy ($Wm^{-2} \cdot \mu m^{-1} \cdot sr^{-1}$)

$i_{\lambda b}$ — spectral intensity of a blackbody ($Wm^{-2} \cdot \mu m^{-1} \cdot sr^{-1}$)

k_{s+g} — the equivalent thermal conductivity of combined solid and gas ($mWm^{-1}K^{-1}$)

k_r — the thermal radiation conductivity ($mWm^{-1}K^{-1}$)

k_t — the equivalent total thermal conductivity ($mWm^{-1}K^{-1}$)

m — the weight of the sample (kg)

n — the refractive index of the medium, eq.(9)

q_{s+g} — the heat flux of combined solid and gas (Wm^{-2})

q_r — radiation heat flux (Wm^{-2})

q_t — total heat flux (Wm^{-2})

S — Coordinate along path of radiation (m)

T — the absolute temperature of the surface (K)

V_b the broken cell volume (m^3)

V_s the volume of solid (m^3)

V_{s+g} the volume of combined solid and gas in the unbroken cell (m^3)

V_t the apparent volume or total volume (m^3)

V_{tb} the volume of all the cells (m^3)

V_{ub} the volume of gas in the unbroken cell (m^3)

Greek symbols

ρ_f apparent density or foam density, (kgm^{-3})

ρ_s the density of the solid, 991.96(kgm^{-3})

ρ_{s+g} the density of the combined solid and gas in the unbroken cells, (kgm^{-3})

σ Stefan-Boltzmann constant, 5.67×10^{-8} ($Wm^{-2}K^{-4}$)

σ_e Rosseland mean extinction coefficient, eq. (8)

$\sigma_{a\lambda}$ spectral absorption coefficient, eq. (13)

$\sigma_{e\lambda}$ spectral extinction coefficient, eq. (13)

$\sigma_{s\lambda}$ spectral scattering coefficient, eq. (13)

τ_λ spectral transmittance, eq. (13)

$\Phi_\lambda(\varpi, \varpi_i)$ phase function

ϕ broken cell ratio, V_b / V_{tb}, eq.(14)

ω solid angle (sr)

ω_i incident solid angle (sr)
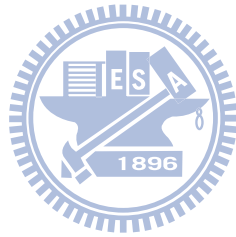
CHAPTER 1

INTRODUCTION

1-1 Overview of Thermal Insulation

The improvement of thermal insulation technology has long been a major issue for researchers who seek reliable and efficient ways of energy conservation. Thermal insulation is a passive energy-saving method that minimizes energy loss during thermal energy storage and transportation. It is widely applied in many modern engineering systems, such as building HVAC, industrial process cooling and refrigeration, cryogenic engineering systems, hydrogen storage, etc. The amount of energy-saving that a good thermal insulation can provide is tremendous. For example, the HVAC loading of a low-temperature logistics center can be reduced by more than 30% using adequate thermal insulation, which consequently reduces the HVAC equipment capacity and energy consumption.

Theoretically, an evacuated metal box can provide excellent thermal insulation because the only heat transport route in an evacuated metal box is thermal radiation. The metal acts as the structural support of the box that is under the pressure difference between ambient atmosphere and vacuum. Nevertheless, the irregular shape of most industrial products has limited the application of evacuated metal box.

Some early HVAC and building insulation applications [1-7] used plate-type insulation

panels that were constituted by fibrous or grainy supporting structure enclosed by sealing bags. Heat transport routes in the plate-type panels include solid conduction through fibers and particles, air convection, air conduction, and radiation. The relatively low thermal conductivity and light-weight of plate-type panels were very attractive for early HVAC and building insulation.

Along with the advancement in foaming technology, closed-cell foams such as PU (polyurethane) and PS (polystyrene) gradually replaced fibrous and grainy materials in insulation applications. Closed-cell foams are superior in several aspects. They are lightweight, low cost, easy to mass produce, and most importantly, without the hazardous effects that fibers and particles could have on human health. Typical closed-cell foams consist of voids, struts, and wall membranes. The voids typically have characteristic length of 1mm and the convection inside the voids is negligible because the Rayleigh number is much lower than 1000, the critical number necessary to initiate natural convection. A typical example of PS foam [8] has an average void size of 400 μm and an effective thermal conductivity of 26 mW/mK at 300K, which consists of contributions by solid conduction (3 mW/mK), gas conduction (19 mW/mK) and radiation (4 mW/mK). Gas conduction in closed-cell foams arises from the gases entrapped inside the cells during foaming process. Figure 1-1 shows the structure of a typical closed-cell PU foam. Although the entrapped gases, which are constituted by the foaming agents such as Chorofluorocarbon (CFCs) and other similar

organic substances, typically have much lower thermal conductivity than air, gas conduction still accounts for most of the heat transfer in closed-cell foams. It is essential for the foaming agents to have adequate diffusivity so that they can diffuse into the cells during foaming process. Nevertheless, the foaming agents also diffuse out the cells after a period of time and is replaced by air, which has higher thermal conductivity and consequently degenerates the insulation performance of closed-cell foam, a phenomenon known as the thermal aging process [3,9]. Furthermore, CFCs are detrimental to the ozone layer. Searching for new foaming agents that have lower environmental impacts and better insulation performance is therefore crucial for the future development of closed-cell foams.

In addition to polymer foams, other materials such as metal foams and ceramic have also been applied in insulation in different temperature ranges. The major issues in high temperature insulation materials are surface oxidation and material sublimation. For low temperature applications, researchers have developed vacuum insulation panel (VIP) technology, see Fig 1-2(b). A VIP is constituted by an open-cell core material that acts as structural support and is enclosed by an impermeable sealing bag. The open-cell structure allows the bag to be evacuated to vacuum to remove all the entrapped air and completely eliminate the heat transfer by air conduction and convection. The effective thermal conductivity could be greatly reduced since only solid conduction and radiation are left in VIP. Commercial VIPs [10-17] have reached thermal conductivity as low as 4~10 mW/mK, about

2 to 6 times lower than closed-cell insulation foams. Three types of VIPs are most common, namely, simple high-vaccum insulation, evacuated porous insulation, and evacuated multilayer insulation, as shown in Fig. 1-2. Figure 1-3 depicts their corresponding effective thermal conductivities.

1-2 Literature Survey

Many researchers remain highly interested in fibrous and grainy insulation materials over the last several decades. Tong and Tien [18-20] predicted radiant heat flux by two-flux and linear anisotropic models to investigate the thermal radiation in fibrous insulation. Comparing with the experimental results obtained by infrared spectrophotometer and guarded-hot-plate apparatus, their model calculation showed consistent results. Chu et al. [21] systematically studied the thermal radiation of ultra-fine powder insulation formed by Aerosil 380 SiO_2 particles with 7nm diameter. If the pore size between the solid particles is lower than the mean free path of air, which is about 20nm at 300K, the diffusive transport of air conduction would be greatly reduced. They concluded that thermal radiation accounts for 10% of the overall effective thermal conductivity at room temperature. The proportion rises to 50% at 1000K. Marge [22] proposed to reduce thermal radiation by adding micro-size powders into foaming materials. Heinemann and Caps [23] thoroughly investigated the optical thickness and thermal radiation of a series of low-density silica aero gel. They

described a numerical technique that precisely predicts the temperature profile and total heat flux in semi-transparent, non-scattering and non-gray media.

The past researches of heat transfer in porous foams can be classified into solid conduction [24-27], gas conduction and convection [8, 28], and radiation [8-57]. Some prominent research results are described below.

Glicksman's group derived thermal radiation of closed-cell foams, as follows. Using cubic model [24-26] and assuming two-third of the membranes and one-third of the struts are parallel to the temperature gradient direction, the solid conduction can be expressed by,

$$k_s = \left(2/3 - f_m/3\right) \times f_s \times k_0 \tag{1}$$

where f_m is the mass fraction of the struts, f_s is solid volume fraction, and k_0 is the thermal conductivity of the solid material. Assuming independent radiation and simulating the closed-cell foam by random arrangement of partially transparent window membranes, a scaled extinction coefficient is given by [29-32],

$$k_r = Q \times 5.23 \times \left(\left(f_m \times f_s\right)^{0.5}/d\right) \tag{2}$$

where Q is efficiency factor and d is average cell size.

Caps et al. [28] studied polyimide foam and proposed a heat transfer model based on the parameters of temperature, pressure and density to calculate gas and solid heat transfer, as well as radiation and overall thermal conductivity. Druma et al. [27] simulated carbon foam by a homogeneous dispersion of spherical voids in a solid matrix and neglected gas and

radiation heat transfer. They investigated heat transfer in carbon foams with different porosity and compared the results of finite element simulation, theoretical solutions, and semi-empirical analysis.

The majority of research papers in foam insulation have been focused on radiation heat transfer. In general, the thermal radiation of foam insulation can be investigated by two approaches [33]: the macroscopic method that uses an inverse technique to retrieve the values of radiation parameters from experimental data, and the microscopic method that analyzes the foam structure from a microscopic point of view to develop predictive models. Several notable researches adopting the macroscopic approach are briefly described below. Larkin and Churchill [34] employed a two-flux model to predict the thermal radiation of Fiberglas, Foamglas and Styrofoam. They presumed an optimal cell diameter in foam materials in terms of minimizing thermal radiation. Arduini and Ponte [35] suggested a solution of equations combining heat conduction and radiation to overcome the nonlinear correlation between thermal radiation and temperature. Giaretto et al. [36] studied the thermal conduction and radiation of open-cell melamine foam insulation. Comparing the measurement results with the prediction by integral model and by diffusive model indicates that the latter is less applicable. Wu et al. [37] investigated the heat transfer of PU foams at 760 torr and 0.014 torr. They concluded that thermal radiation accounts for 20% of the heat transfer at 0.014 torr. They also discussed that organic gases were released within VIP after a long period of operation and

absorbents were required to absorb the gases and maintain low thermal conductivity. Li [38] proposed a conjugate gradient method to solve the inverse conduction-radiation problem for simultaneous estimation of the single scattering albedo, the optical thickness, the conduction-to-radiation parameter, and the scattering phase function. The single scattering albedo and the optical thickness can be estimated accurately from both exact and noisy data.

For microscopic approach, the following researches are notable and worth mentioning. Doermann and Sacadura [39] adopted a dodecahedron cell structure to simulate foaming materials and used a weighted scattering coefficient for anisotropic scattering to correct the Rosseland mean extinction coefficient. For carbon foam in high temperature applications, their model provides a better prediction of thermal radiation than earlier models. Kamiuto [40] adopted the Dul'nev cubic unit cell model to predict the thermal and radiative properties of open-cellular porous materials for applications in high-temperature heat transfer augmentations. Quenard and Giraud [41] developed an experimental procedure to measure the micro-structural geometrical parameters of a packing of cellular pellets such as EPS foam. They concluded that a critical value of foam density exists for any given cell size to minimize effective thermal conductivity. Baillis et al. [42] used the predictive model developed by Doemann and Sacadura that incorporates the minimum/maximum strut thickness and foam porosity. Their accurate description of foam geometry allows an estimation of the spectral radiative properties of open-cell foam insulation. Following this research, the realistic

simulation of foam geometry attracted a lot of interests. Lu et al.[43] developed a simple

cubic unit cell model to explore the applications of open-cell metal foam in compact heat

exchangers. Nevertheless, their prediction led to an overestimate result. Zhao et al. [44-45]

measured the radiative heat transfer of FeCrAlY alloy foams having high porosity (larger than

95%) and various cell diameters. The extinction coefficient decreases along with the increase

of cell diameter, which has little influence on reflectivity. Both the extinction coefficient and

reflectivity were found to increase as the operation temperature increased. Micco and Aldao

[46] derived radiative heat transfer rates using a geometrical model and concluded that the

geometrical model produces results more consistent with experimental data than the

derivation based on Rosseland mean extinction coefficient. Coquard and Baillis [47]

simulated the closed-cell structure of EPS by dodecahedrons and cubes. By solving

one-dimensional steady state coupling equations of radiative and conductive transfer, they

found the following parameters pertinent to heat transfer, which are listed in order from

higher influence to lower influence: foam density, mean cell diameter, inter-bead porosity,

and mean bead diameter. Wang and Pan [48] developed a random generation-growth method

for reproducing the microstructures of open-cell foam by using periodic arrays with regular

geometries. Due to high porosity, low thermal conductivity of each component, and

non-negligible radiative heat transfer, the predicted thermal conductivity is lower than the

experimental data. Placido et al. [33] and Kuhn et al. [8] proposed a porous structural model

that is based on cylindrical struts, pentagon membranes, and dodecahedron cell. Their analysis of solid and gaseous heat transfer followed the model proposed by Schuetz and Glicksmann [25] and Caps et al. [28]. Many earlier studies simulated the complex cell geometry of porous foams by simplified regular cell models and had been focused on polymer foams having relatively high density. For low density foams, the model prediction results are not as good in terms of comparing with experimental data. To some degree, it can be explained by the fact that many earlier studies relied on a single parameter to evaluate thermal radiation, namely, the weighted Rosseland extinction coefficient, which is not enough to describe all thermal radiation properties of low density foaming materials.

To obtain more precise prediction of thermal radiative properties, some earlier studies have employed tomography scanning technique to study the cell structure of foaming materials. Zeghondy et al. [49, 50] were the first to utilized X-ray scanning technique to acquire the information of cell structure and applied it in thermal radiation calculation. They employed the technique of Radiative Distribution Function Identification (RDFI), which was developed by Tancrez and Taine[51], to obtain the structure of open-cell foams. Comparing with experimentally measured reflectance, the data of a semi-transparent homogeneous material showed excellent consistency. In the case of aluminum foams, Loretz et al. [52] used geometric optics law to model the interaction of radiation with the particles forming the foam for estimating the extinction, the scattering albedo and the scattering phase function. Unlike

the model of Glicksman and Torpey that neglects the scattering effect, the scattering of the aluminum foam is normally modeled by opaque spheres with diffusive reflection, because the high reflectivity of aluminum metal makes scattering an indispensible part in describing the radiative characteristics of the foam.

To summarize, many models based on regular-shaped cell assumption have been proposed in earlier studies, but their application to low-density irregular shaped foams, especially those partially-open-cell foams, is questionable. The x-ray scattering technique provides another approach to reveal the detailed transport in porous foams. It is, however, specific to individual cases and does not provide general guidelines for material improvement.
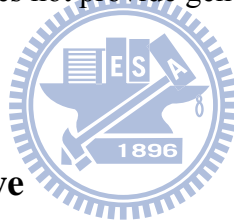
1-3 Motivation and Objective

In open-cell foams, a cell breaks when forming agents induce enough internal pressure to overcome the cell membrane strength, which depends largely on the viscosity of the material, and therefore on the glass transition temperature (T_g). The material viscosity is relatively high at temperatures above T_g, but the material hardens immediately when the temperature falls below T_g. Both features hinder the cell from breaking. It is very difficult to control the material temperature and simultaneously break all the cells inside the material. The positions and number of the unbroken, i.e., closed, cells are hard to control. Nevertheless, cell geometry, including the struts and the residue membranes, plays a key role in both solid conduction and

thermal radiation in VIPs. Further enhancement of VIP performance requires determining the influence of cell geometry on conduction and radiation, and using this knowledge to improve the manufacturing process.

Because of the complex structural geometry of open-cell core material in VIP, most of the previous studies assumed all closed-cell or all open-cell structures in their analyses. However, practical applications are far more complicated since the cells in VIPs are not 100% broken, which means that some cells are closed. Due to the lack of systematic experimental data of partially-open-cell structure, it is difficult to verify the model prediction even using cell structure obtained by tomography scanning. The purpose of the present study is to systematically investigate partially-open-cell foams as the core materials in VIP. Appropriate macroscopic parameters, such as broken cell ratio, solid volume ratio, and average cell size, will be identified to characterize the foam performance, which will form a basis for future researches of cell morphology in thermal radiation. This study therefore deals with heat transfer in VIPs with partially open cell structures, focusing on VIPs with most of the cells broken. Specifically, more than 90% of the cells are broken and less than 10% of the cells are closed. This high ratio of broken cells is necessary and common in VIPs with satisfactory performance.

Chapter 2 reports a mathematical modeling of partially open polystyrene foam. The total heat flux is divided into the transfer by conduction of solid and gas, and by radiation. The

effective thermal conductivity consists of the equivalent thermal conductivity by combined solid and gas, and the equivalent thermal conductivity by radiation. Because all the samples are optically thick, the radiative conductivity can be calculated by Rosseland mean coefficient. In the mean time, this study proposed a new parameter of broken cell ratio to describe open cell content. Together with the parameter of specific solid volume ratio, the geometric influence on extinction coefficient can be clearly manifested.

Chapter 3 describes the preparation of samples, air pycnometer, Fourier transform infrared spectrometer, and guarded-hot-plate system. This chapter also includes the uncertainty analysis of effective total thermal conductivity.

Chapter 4 studies the relationship between broken cell ratio, solid volume ratio and cell size, and their effects on heat transfer mechanisms. A total of 14 samples with different cell geometries were produced, and their heat transfer rates were measured and analyzed. The results will be helpful in describing heat transfer in VIPs and serve as a basis for improving VIP performance in the future. Besides, Chapter 4 also explores the effects of polythene additive on the performance of PS vacuum insulation panels. A total of 42 samples with different PE contents, namely, 0wt%, 2wt% and 5wt%, were fabricated in this study. Their heat transfer rates were measured and analyzed. The results will be helpful in manufacturing VIP with improved performance.

The last chapter gives a conclusion of this study and a recommendation for future

research directions.
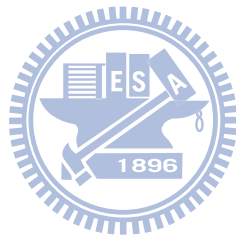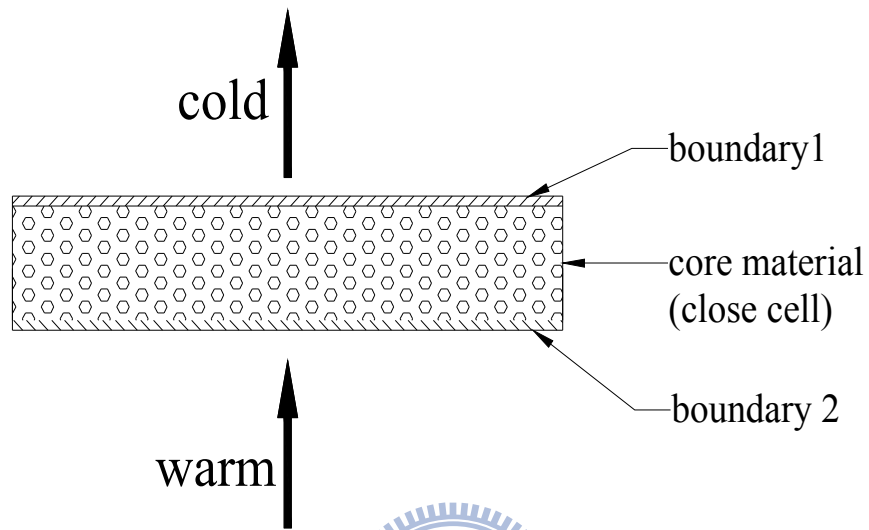
Fig.1-1 The structure of closed cell foam [1]
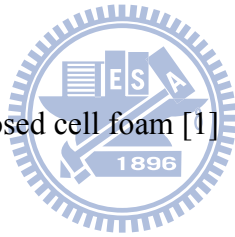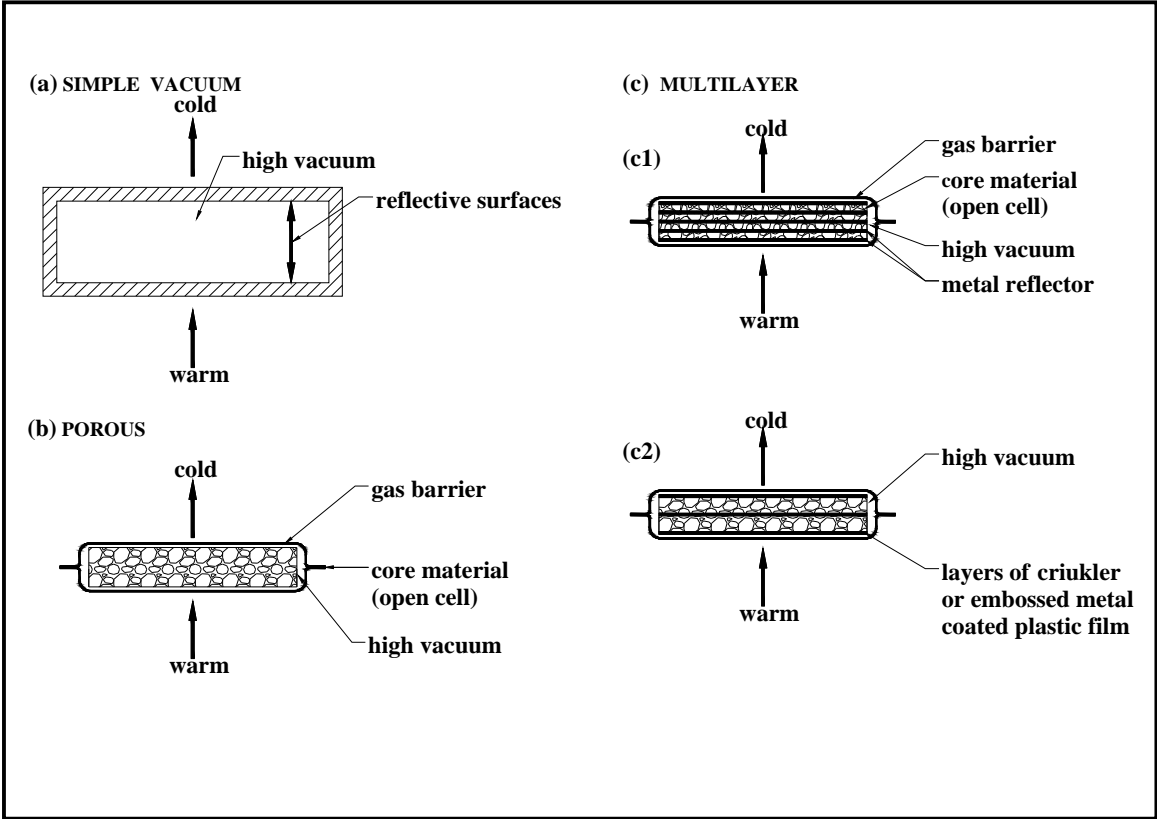
Fig.1-2. Various types of cryogenic insulations [1]
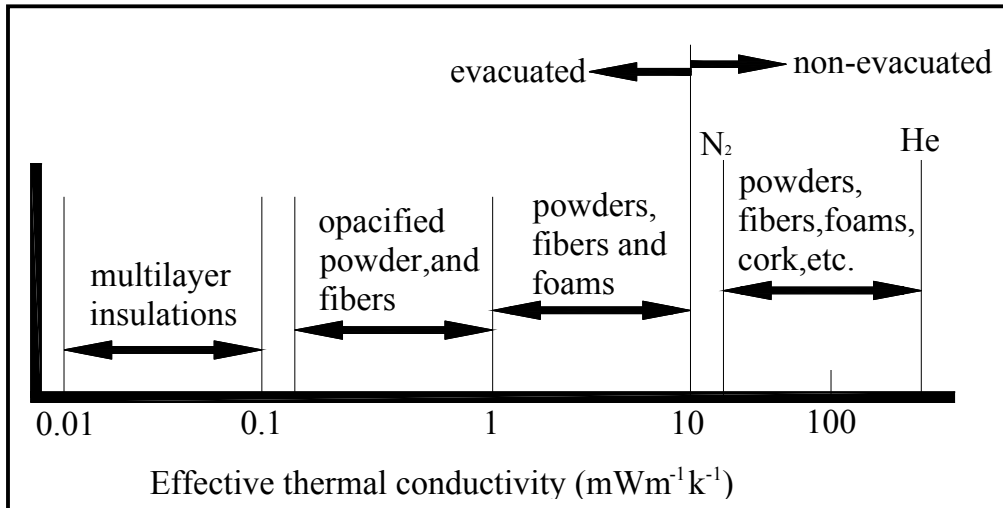
Fig.1-3. Thermal conductivity of cryogenic insulation. Note: Forms are open cell type between $1(mWm^{-1}K^{-1})$ to $10(mWm^{-1}K^{-1})$ [1].
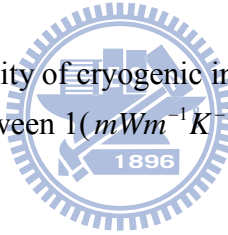
CHAPTER 2

THEORY

2-1 Combined Solid Conduction and Thermal Radiation

2-1-1 Assumptions

The core material of PS foam has a partial open-cell porous structure. Heat transferred through VIP via two mechanisms: (1) conduction by gas and solid; and (2) by radiation. The one-dimensional, steady state energy equation for a participating medium with no internal heat generation is considered in this study. It is further assumed that $k_s \approx k_{s+g}$ since the contribution by gas conduction is relative small in the samples with broken cell ratio higher than 90%. Note that the heating before sealing and evacuating also helped to eliminate the gases enclosed in closed cells.

The solid volume fractions of the samples are normally less than 0.6. For the solid phase, over 97% material is polystyrene, which has a refractive index of 1.55. Therefore, if one estimates the refractive index (n) of the foam by weighing the ratio of solid to void volume, the result would be around 1.03, which is very close to the refractive index of air and vacuum and is neglected in the calculation. The dimensionless optical thickness of a PS sample is evaluated by multiplying its geometrical thickness by its mean extinction coefficient [58-59].

2-1-2 Limitations

The samples in this study normally operate in the temperature range of 0 to 30 and

without heat generation within the core material. Contact thermal resistance between envelope

and core material is considered part of the solid conduction and is not distinguished from it in

this study. This simplification does not influence the measurement accuracy or the

determination of total thermal conductivity, because the contact surface is under a

compression force exerted by the atmospheric pressure and the contact resistance is relatively

constant for a given sample.

In this study, thermal radiation and total heat transfer are measured experimentally. Solid

conduction is determined by deducting thermal radiation from total heat transfer, as described

in Eq.(4). Theoretically, it is also possible to measure solid conduction and determine thermal

radiation by deducting solid conduction from total heat transfer. Nevertheless, the uncertainty

of determining thermal radiation indirectly is likely to be larger. This is manifested by

assuming an equal uncertainty percentage in measuring thermal radiation and solid

conduction. The influence on thermal radiation uncertainty by solid conduction uncertainty is

higher because the former accounts for less than 20% of the total heat transfer. An 1%

uncertainty in solid conduction represents an 4% uncertainty in thermal radiation.

2-1-3 Equivalent Total Thermal Conductivity

The heat flux (q_t) in VIPs can be divided into the transfer by conduction of solid and gas

(q_{s+g}), and by radiation (q_r),

$$q_t = \left(q_r + q_{s+g}\right) \tag{3}$$

The concept of equivalent thermal conductivity applies,

$$k_t = k_r + k_{s+g} \tag{4}$$

where k_t is the equivalent total thermal conductivity, k_r is the fraction of equivalent thermal conductivity induced by thermal radiation, and k_{s+g} is the equivalent thermal conductivity of combined solid and gas.

2-1-4 Equivalent Thermal Conductivity by Radiation

The contribution to the equivalent thermal conductivity by radiation is evaluated by the following method. A medium is considered optically thick, if its optical thickness is far greater than 1. Since all the measured optical thickness of this study's samples exceeded 45, it is satisfactory to assume all samples are optically thick and use Rosseland mean coefficient .

For the diffusion approximation, the total net radiative heat flux of an absorbing, emitting, and isotropic scattering medium can be written as [37, 58-59],

$$q_r = -\frac{4\pi}{3} \int_{\lambda=0}^{\infty} \frac{1}{\sigma_{e\lambda}} \frac{de_{\lambda b}[T(S)]}{dS} d\lambda \tag{5}$$

The derivate of $e_{\lambda b}[T(S)]$ with respect to S can be written as

$$\frac{de_{\lambda b}}{dS} = \frac{de_{\lambda b}(T)}{de_b(T)} \frac{de_b(T)}{dS} . \tag{6}$$

Substituting Eq. (8) into Eq. (7), the equation of radiative flux is obtained by

$$q_r = -\frac{4\pi}{3} \frac{de_b(T)}{dS} \int_{\lambda=0}^{\infty} \frac{1}{\sigma_{e\lambda}} \frac{de_{\lambda b}(T)}{de_b(T)} d\lambda .$$

(7)

The Rosseland mean extinction coefficient, σ_e, is defined as [58-59]

$$\frac{1}{\sigma_e} = \int_0^{\infty} \frac{1}{\sigma_{e\lambda}} \frac{de_{\lambda b}}{de_b} d\lambda .$$

(8)

Since

$$e_b(T) = \frac{n^2 \sigma T^4}{\pi}$$

(9)

where n is the refractive index of the medium and σ is the Stefan-Boltzmann constant, for

constant n, Eq. (9) can be written as

$$q_r = -k_r(T) \frac{dT(S)}{dS}$$

(10)

and the equivalent thermal conductivity for radiation is defined as

$$k_r = \frac{16 n^2 \sigma T_m^3}{3\sigma_e}$$

(11)

where T_m is the arithmetic mean of the boundary temperatures.

The mean extinction coefficient, σ_e, can be related to the transmittance of the media, as

follows. The radiative heat transfer in an one-dimensional homogeneous planar system is

described by [59]

$$\frac{di_\lambda}{dS} = -[\sigma_{a\lambda}(S) + \sigma_{s\lambda}(S)] \times i_\lambda(S) + \sigma_{a\lambda}(S) \times i_{\lambda b}(S)$$
$$+ \frac{\sigma_{s\lambda}}{4\pi} \int_{\omega_i=0}^{4\pi} i_\lambda(S, \omega_i) \Phi_\lambda(\omega, \omega_i) d\omega_i$$

(12)

where i_λ is the spectral intensity of thermal radiation.

For the case of a cold homogeneous medium, the emission terms and in-scattering terms

are negligible under the influence of a relatively strong but unidirectional beam of radiant

energy. The solution is Eq.(5) given by Beer's law, and a transmittance is defined by [59]

$$\tau_\lambda \equiv \exp(-\sigma_{e\lambda} \cdot \Delta S) \tag{13}$$

where $\sigma_{e\lambda} = (\sigma_{a\lambda} + \sigma_{s\lambda})$ is the spectral extinction coefficient. The equivalent thermal conductivity of radiation, k_r, can be experimentally determined by Eq.(13), (8), and (11), as described in Sec. 3-2-3.

2-2 Foam Parameters of Partial Open Polystyrene Foam

2-2-1 Broken Cell Ratio

To further distinguish the contribution by solid and by gas, this study introduces a broken cell ratio, ϕ, representing the ratio of broken cell volume to the total cell volume

$$\phi = \frac{V_b}{V_{tb}} = \frac{V_t - \dfrac{m}{\rho_{s+g}}}{V_t - \dfrac{m}{\rho_s}} = \frac{\dfrac{m}{\rho_f} - \dfrac{m}{\rho_{s+g}}}{\dfrac{m}{\rho_f} - \dfrac{m}{\rho_s}} = \frac{\rho_s}{\rho_{s+g}} \frac{(\rho_{s+g} - \rho_f)}{(\rho_s - \rho_f)} \tag{14}$$

where m is the mass of the sample, V_t is the apparent volume (total volume), V_s is the volume of solid, V_{s+g} is the volume of combined solid and gas in the unbroken cell, V_{ub} is the volume of gas in the unbroken cell, V_b is the vacuum volume inside the VIP (which actually contains air in extremely low pressure) or the broken cell volume, and V_{tb} is the volume of all the cells. The apparent density, or foam density, $\rho_f = m/V_t$, was measured using the ASTM D-1622 method. The value $\rho_{s+g} = m / V_{s+g} = m / (V_{ub} + V_s)$ is the density of the combined solid and gas in the unbroken cells. Note that this approach disgards the mass of extremely low-pressure gas in the vacuum. Subtracting the broken cell volume from the total

volume produces V_{s+g}. The former was measured by an AccuPyc 1330 Pycnometer with an accuracy of 0.03 %. The term ρ_s is the density of the solid, taken as the density of the raw polystyrene, which is $991.96\,(kgm^{-3})$.

2-2-2 Solid Volume Fraction

The solid volume fraction, f_s, is the ratio of solid volume to the total volume and is readily obtained by dividing the foam density of the sample by the polystyrene density.

$$f_s = \frac{V_s}{V_t} = 1 - \frac{(1 - f_{s+g})}{\phi} \qquad (15)$$
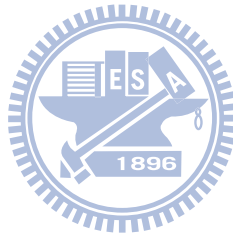
CHAPTER 3

EXPERIMENTS

3-1 Sample Description

The samples were prepared by the following procedure. A mixture of polystyrene, polyethylene, carbon black, and calcium stearate were put into a batch die of 400mm diameter and subjected to a 40-ton press. A photo picture of the die and the press equipment is shown in Fig. 3-1. After mixing with the molten mixture, foaming was performed by introducing CO_2 and R-134a into the die to form a supercritical fluid. The high pressure gas in the die was released after 6 hours, forming a plain board measuring 250mm long × 250mm wide × 6~26mm thick. After about an hour of heating, the material was enclosed by a metal foil envelope, which was sealed after the enclosed air was evacuated to 10^{-4}torr. The photo picture is shown as Fig.3-2 Experiments were designed to vary the cell geometry of the samples by modulating die temperature and gas pressure. Die temperature is controlled by heaters and is maintained at a fixed temperature with a stability of ±0.5C throughout the process. Figure 3-3 shows the dual pressure control system that was able to separately control the pressure and the amount of CO2 and R-134a. During the forming process, the gas pressure normally ranged between 2500psi and 3300psi.

3-2 Apparatus

3-2-1 Air Pycnometer

The operation principle of air pycnometer is followed in accord with Boyle's law

depicted the relationship that a increase in pressure of a confined gas should be proportional

to decrease in volume. The simplest type of air pycnometer essentially has two identical

equal-volume cylinders and pistons, A and B as shown Fig.3-4. The photo picture can be seen

in Fig.3-5. The cylinder B inserted a sample of PS foam. Pistons in both cylinders allow

volume change.   When a sample of PS foam appears in the cylinder B, the decreased the

volumes results in the increased pressure. With the extent of this difference, the method of air

pynometer can determine numerical values for the percentage of volume occupied by open

cell PS foam. Detailed calculation procedure can take it reference as D 2856-70 Standard Test

method.
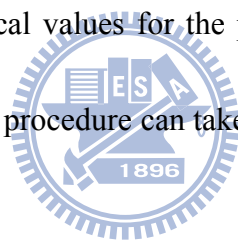
3-2-2 Fourier Transform Infrared (FTIR) Spectrometer

A Perkin-Elmer Spectrum 2000 Fourier Transform Infrared Spectrometer was used to

measure the infra-red transmission of the foam insulation specimen. The infra-red

transmission apparatus are made up of three basic parts   the light source unit, a spectral

radiation detector, and the sample cell. A deuterated triglycine sulfate (DTGS) with a

pyroelectric bolometer standard is using as the detector. It is noted that the spectrometer needs

nitrogen gas to purge and KBr windows to seal. KBr is the beam-splitter. A reference signal

generated by a plane-polarized single mode He-Ne laser at 632.8 nm with Si-diode detection

empowers the spectrometer electronics to sample the interferogram at precise intervals. Fig. 3-6 is a schematic diagram illustrating the basic system. The photo picture of FTIR is shown in Fig. 3-7. This spectrometer is the type using mechanical bearing of a fast scanning Michelson interferometer which consists of a fixed mirror, a movable mirror, and a beam-splitter. Beam-splitter equally divides the incident radiation into two beams. One transmits to the moving mirror and the other reflects to the fixed mirror. Then, these two beams are reflected from the mirrors back to the beam-splitter and recombine. Due to the two beams travel different distances before recombining, an optical difference occurs. Because of the position of moving mirror and the frequency of the retardation, it generates a pattern of constructive and destructive interference. The varying optical path difference can be obtained from the moving mirror which is driven at a constant velocity by a linear motor under computer control. An interference pattern is obtained as the path difference. Finally, the combined beam traverses the specimen to reach the detector. It converts the interferogram into a single-beam spectrum by using a Fourier transform in the computer.

To begin the experiments, the specimen of PS foam is cut to less than monocellular thickness. The heat flow direction of all specimens is perpendicular to the cutting planes. The thickness of specimen is measured by micrometer gauge as shown in Fig.3-8.

The average cell size of each sample was calculated by a method in accordance with ASTM standard D 3576-77, using a SEM picture of the sample.

3-2-3 Guarded-Hot-Plate System

The Guarded-Hot-plate System made by EKO Instruments trading company (model HC-072) is used to measure the equivalent total thermal conductivity of VIP at 10^{-4} torr. The photo picture and schematic diagram of the guarded hot plate system are shown as Fig.3-9 and Fig. 3-10, respectively. The Guarded-Hot-plate System consists of thickness measurement sensor, hot and cold plates and heat-flow meter. Due to the effect of edge heat losses and to the thermal unbalance between test section and guard ring, it is very important to treat the specimen thickness and the hot plate dimensions (guard and gap width, side) in order to less affect the errors in the measurement of thermal conductivity. The heat flow meter is a simple, rapid and accurate device to sense that heat passes through the quantities of VIP. The relative specification needs consult the standard of ASTM C518 and JIS 1412. Before experiment, the sample of VIP places between two flat plates maintained at different temperature. Then, the difference temperature between hot plate and cold plate sets approximately $30^o K$. The heat flow meter and the copper-constantan thermocouples were mounted on the center of hot and cold plates to sense the heat and the temperature. Using P.I.D. digital heater controls temperature of hot and cold plates. Besides, the cold plate is cooled by a 400W air cooling compressor type chiller. The standard reference material (SRM) 1450B fibrous glass board [60] has been used to individually calibrate the temperature measuring device.

The spectrum transmittances of the samples were measured by a Perkin Spectrum 2000 Fourier Transform Infrared Spectrometer. For the measurement, a thinly sliced foam specimen was subjected to normal incident irradiation in the wavelength range of 2.5 to 25 μm. The specimen was first put into an oven to remove its moisture and volatile organic gas contents. With the measured transmittance, the spectral extinction coefficient is calculated by Eq. (13). The term σ_e is then calculated by substituting $\sigma_{e\lambda}$ into Eq. (8) and k_r is subsequently obtained by Eq. (11). With the knowledge of k_r and k_t, k_{s+g} can be inferred from Eq. (4). Note that k_r and k_{s+g} reveal the contribution by radiation and combined solid and gas, respectively.
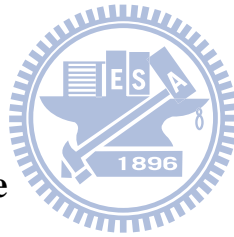
3-3 Experimental Procedure

The estimation of cell size based on the principle of ASTM D 3576-77 (Standard test method for cell size of rigid cellular plastics) is briefly described as below. Three equally-spaced parallel lines and three equally-spaced vertical lines were plotted on the SEM picture of the sample. Their lengths (in μm) were measured by a ruler. The line length divided by the number of the cell counted along the line to obtain cell chord length. Average cell chord length was calculated based on the information obtained from all the line. The averaged cell size was then calculated by the relationship between cell size (cell diameter) and cell chord length assuming spherical cell shape.

Broken cell ratio was directly estimated by the density of solid, foam and combined solid

and gas in the unbroken cells with eq. (14). The density of solid is taken as the density of the raw polystyrene, which is 991.96(kgm^{-3}). The density of foam is obtained by dividing the sample weight by its total volume. To obtain the density of combined solid and gas in the unbroken cells, which is defined by ρ_{s+g} ($= m / V_{s+g} = m / (V_{ub} + V_s)$), the combined volume of unbroken cell and solid ($V_{ub} + V_s$) was first measured by an AccuPyc 1330 Pycnometer. The AccuPyc 1330 Pycnometer consists of a sample volume cup (cylinder B), a valve (Valve B) and an expansion volume device (Cylinder A) as shown in Fig.3-4. After a testing sample was put into the sample volume cup, the system started to evacuate to below 0.1 torr. Piston A and Piston B came to position 2 and Valve B was closed. Helium gas then filled into the expansion volume device and Piston A moved to be position 1. A reference hand-wheel was used to push the piston A back to the position 2. When the Valve B was opened, Helium gas diffused into the Cylinder B. Because the testing sample adsorbed Helium within the voids of the broken cells, Piston B moved to position 3. The volume between position 2 and position 3 was then the desired volume ($V_{ub} + V_s$). The weight (m) was measured by mass balance. Finally, f_{s+g} was obtained by dividing ($V_{ub} + V_s$) by V_t. Substituting f_{s+g} and ϕ into the eq.(15) led to f_s.

3-4 Uncertainty Analysis

The equivalent total thermal conductivity (k_t) was measured by a commercial thermal conductivity meter (EKO HC-072), which was designed in accordance with industrial

standards JIS A 1412 and ASTM 518. The device consists of a hot and a cold plate, thin film

heat-flow meters and a thickness measurement sensor. The temperature of center of hot and

cold plates was measured by the thermocouples. The 250mm long × 250mm wide ×

(6~26)mm thick samples were clapped between the hot and the cold plate with integrated heat

flow meters. The following formula is used to the thermal equivalent conductivity,

$$k_t = \frac{E \cdot L}{S \cdot \Delta T}$$

where S is the sensitivity of heat-flow meter, ΔT is the temperature difference between

the hot and the cold plate, E is the output of heat-flow meters, and L is the thickness of

the sample. The uncertainty is estimated based on the data of sample L_3,

$$\delta k = \left[\left(\frac{k_t}{q_t}\right)^2 \delta q_t^2 + \left(\frac{k_t}{s}\right)^2 \delta s^2 + \left(\frac{k_t}{\Delta T}\right)^2 \delta \Delta T^2 \right]^{0.5}$$

$$\delta k = \left[\left(\frac{6.6}{23.34}\right)^2 (0.02)^2 + \left(\frac{6.6}{0.00646}\right)^2 (0.00005)^2 + \left(\frac{6.6}{22.8}\right)^2 \right]^{0.5}$$

$$= 0.05896 (mW / mK)$$

Therefore, the equivalent total thermal conductivity can be calculated by,

$(\delta k / k_t) = (0.05896 / 6.6) = 0.0089$. That is, the uncertainty of measuring specimen total

thermal conductivity can be controlled to within 0.89%, as estimated by the method of Wu et

al. [37].

Fig.3-1. The picture of the 40 tons press equipment and the 400mm diameter mold.
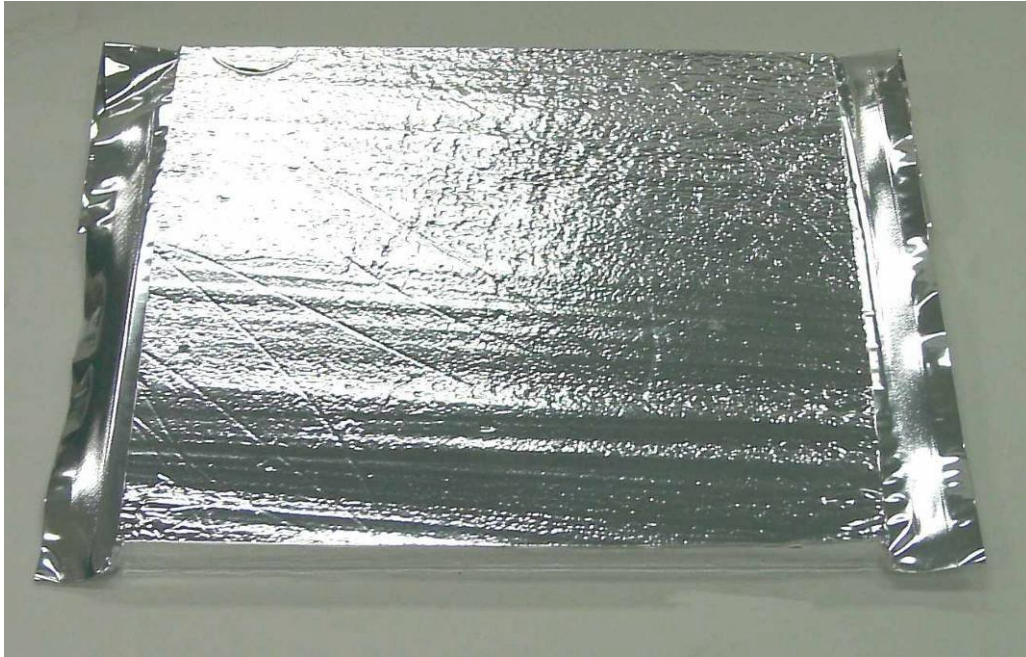
Fig.3-2. Sample of VIP with Polystyrene Form
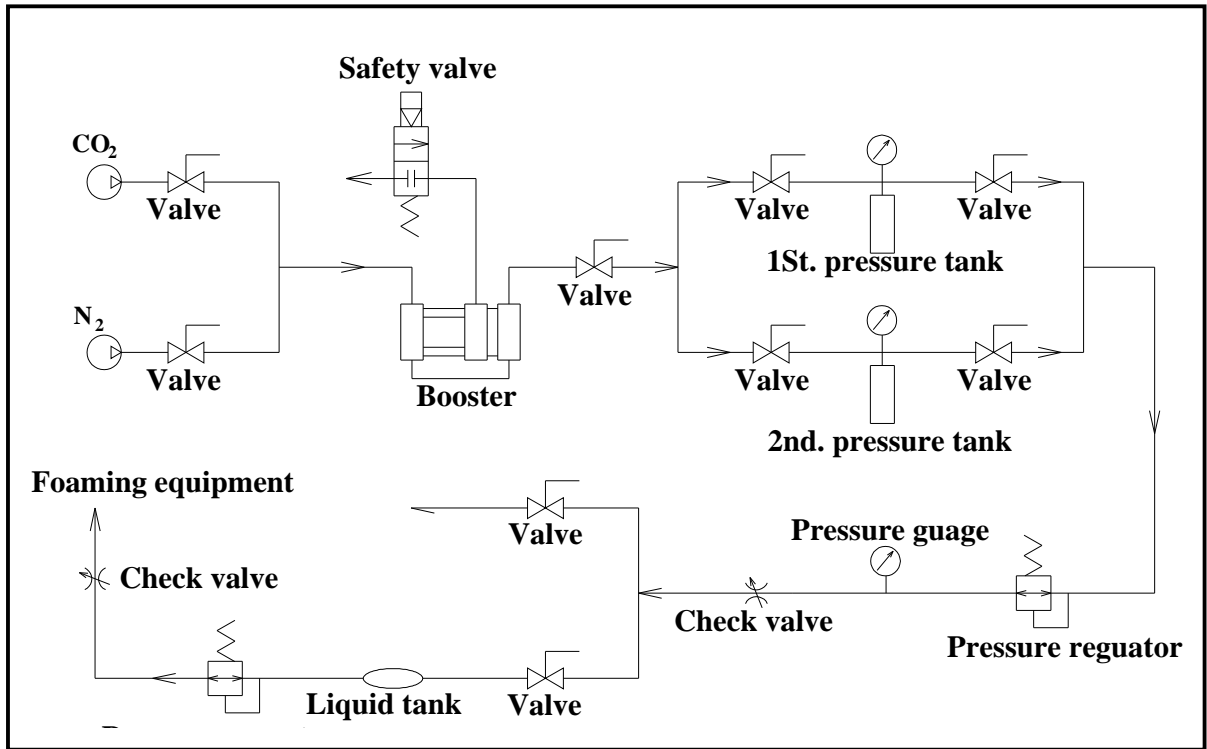
Fig.3-3. The dual pressure control system used to modulate the foaming pressure.
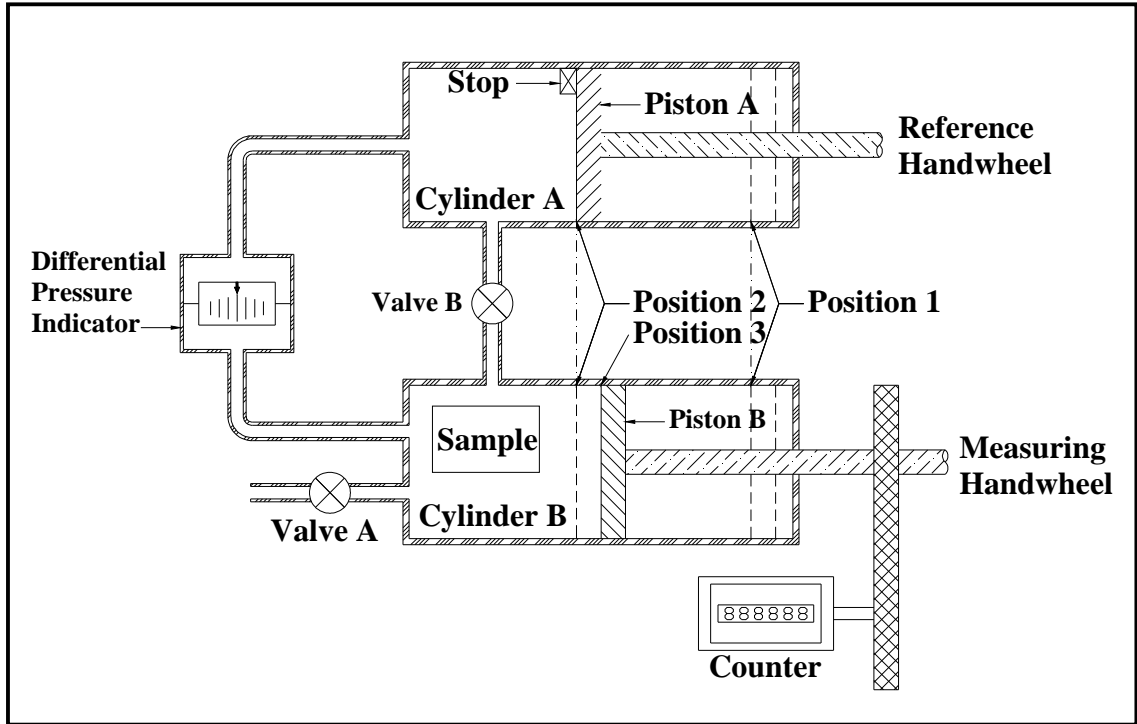
Fig.3-4. Schematic diagram of Air Pycnometer

Fig.3-5. Photo picture of Air Pycnometer
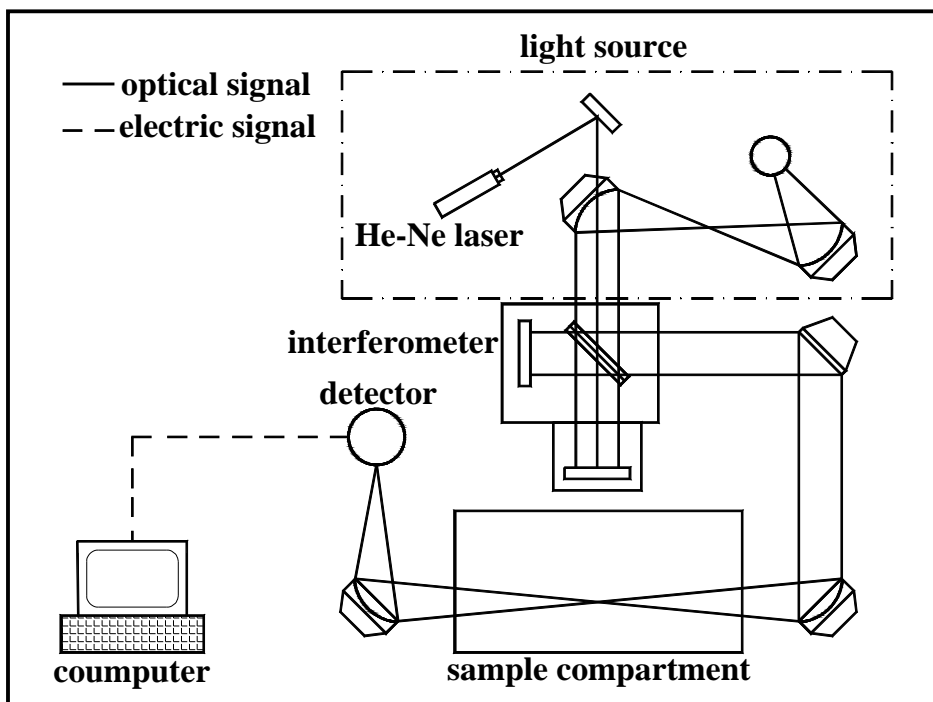
Fig. 3-6 Schematic diagram of the Fourier Transform Infrared Spectrometer

Fig. 3-7 Photo picture of the Fourier Transform Infrared Spectrometer
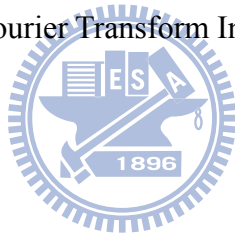
Fig.3-8. Photo picture of micrometer gauge

Fig.3-9. Photo picture of equivalent total thermal conductivity measurement system
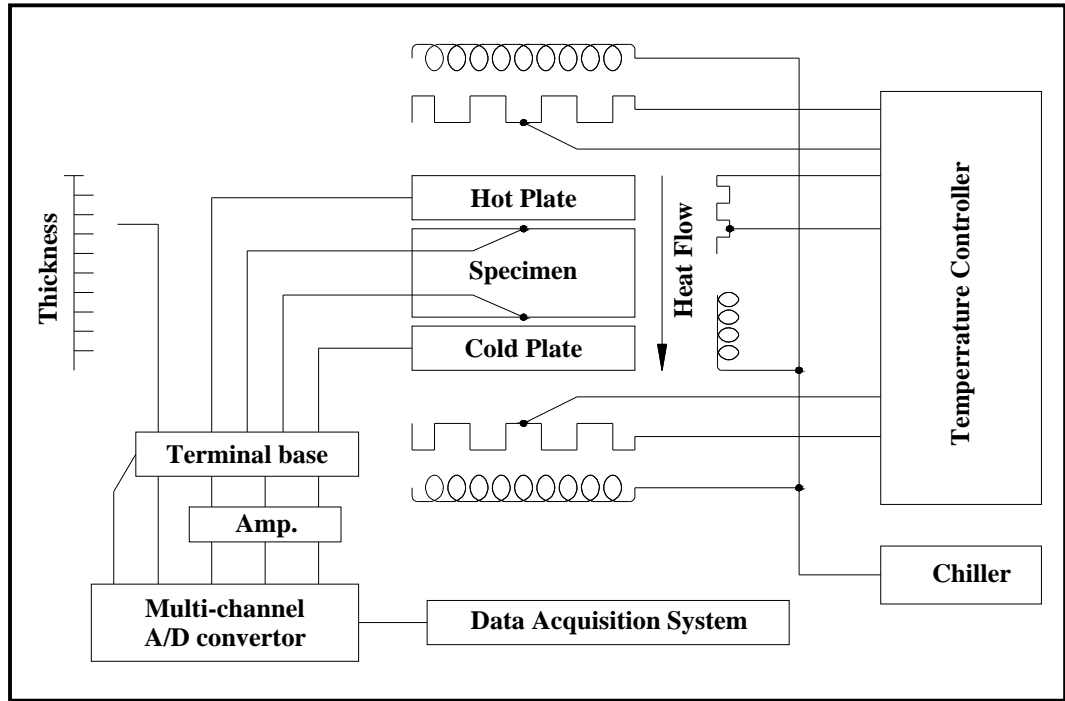
Fig.3-10. Schematic diagram of equivalent total thermal conductivity measurement system

CHAPTER 4

RESULTS AND DISCUSSION

4-1 Polystyrene Foam Vacuum Insulation Panels

Figure 4-1 shows a SEM picture of the material sample. The structure typically consists of struts, cell membranes, broken cells, and unbroken cells. A total of 14 samples were produced for analysis in this study, all with partially open cell structures and broken cell ratios (see the definition below) ranging from 90% to 98%.

Table 4-1 summarizes the measurement results of the 14 samples. The samples fall into two distinct groups with different solid volume fraction. The first group has a lower solid volume fraction (referred to as LSFG) and includes L1 to L6 with $0.0413 < f_s < 0.0494$. The second group has a higher solid volume fraction (referred to as HSFG) and includes H1 to H8 with $0.0615 < f_s < 0.0706$. The variation of solid volume fraction exerts a profound influence on VIP heat transfer, as explained later. Figures 4-2 and 4-3 show examples of spectral transmittance and spectral extinction coefficient, respectively. Note that this spectrum does not reveal CO_2 absorption, which could occur at $2.7\,\mu m$, $4.3\,\mu m$, $9.4\,\mu m$, $10.4\,\mu m$, and $15\,\mu m$, or H_2O absorption, which could occur at $2.7\,\mu m$ and $6.3\,\mu m$. This indicates that the amount of CO_2 and H_2O trapped in the unbroken cells is insignificant in terms of influencing radiation heat transfer. This is reasonable since most of the cells in the samples are broken and evacuated.

4-1-1 The Relationship Description of Physical Properties

Figure 4-4 plots the broken cell ratio versus the cell size of the 14 samples. The data

visibly falls into two groups based on the solid volume fraction. The HSFG cell sizes are

typically larger than LSFG cell sizes. Both groups show an almost linear dependence of cell

size on open cell ratio. The trend in Fig. 4-4 can be explained by the fact that a higher solid

volume enables the cells to expand further before they are broken, and therefore they have a

larger cell size after foaming. On the other hand, to obtain a higher broken cell ratio, some of

the unbroken cells must be expanded further until they are broken. Consequently, this also

increases the average cell size.
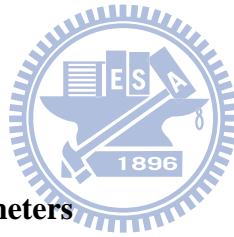
4-1-2 The Effects of Foam parameters

Figures 4-5 and 4-6 plots the Rosseland mean extinction coefficient data against

variations in cell size and broken cell ratio, respectively. All the extinction coefficient data

falls into a single straight line when plotted against the broken cell ratio, as Fig. 4-06 shows.

This indicates that the broken cell ratio is the dominant factor in determining the extinction

coefficient. The VIP extinction coefficient consists of two parts, the absorption part, σ_α, and

the scattering part, σ_s, that is, $\sigma_e = \sigma_\alpha + \sigma_s$. The former represents the absorption effect of

solid material and depends largely on the solid volume fraction. The latter is affected by the

geometry of the porous foam structure, which is characterized by the average cell size and the

broken cell ratio. For the 14 samples investigated in this study, the solid volume fraction plays

a minor role in determining the extinction coefficient, as Fig. 4-6 indicates. The group with a

higher solid volume fraction exhibits only a slight increase in extinction coefficient compared

with the lower solid volume fraction group, although the average solid volume fractions of the

two groups differ by more than 44% (0.045 to 0.065). This can be explained by the fact that

the solid volume fraction of the samples is so small that the extinction is dominated by

scattering and the contribution of absorption is insignificant. The apparent dependence of

extinction coefficient on cell size, as Fig. 4-5 shows, could be interpreted as the dependence

on broken cell ratio, since cell size and broken cell ratio are well correlated under a specific

volume fraction, as Fig. 4-4 indicates.
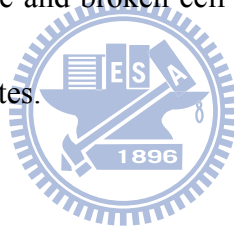
4-1-3 The Influences of Lower Solid Fraction

Figure 4-7 shows the equivalent thermal conductivities of the lower solid volume group,

including the total thermal conductivity, k_t, the thermal conductivity by solid conduction, k_s,

and the equivalent thermal conductivity by radiation, k_r. Figure 4-7 shows that as the cell

size decreases, which creates more conduction transport routes in the solid material, solid

conduction increases. On the other hand, radiation decreases as the cell size decreases. Note

that the decrease in radiation (increase in extinction coefficient) is attributable to the change

in broken cell ratio, as explained earlier. Consequently, there is a best cell size (best broken

cell ratio), which produces the lowest total thermal conductivity after combining k_s and k_r.

In Fig. 4-7, the lowest total thermal conductivity is around 6.5 ($mWm^{-1}K^{-1}$), which occurs at

a broken cell ratio of approximately 0.95 and corresponds to a cell size of about 120 μm.

4-1-4 The Influences of Higher Solid Fraction

Figure 4-8 shows the thermal conductivities of the higher solid volume fraction group,

with a trend similar to that in Fig. 4-7. The best broken cell ratio falls at around 0.97,

corresponding to a cell size of 300 μm, and results in the lowest total thermal conductivity of

7.6 ($mWm^{-1}K^{-1}$). Similar dependence of total thermal conductivity on cell size is found in the

simulation work by Placido et al. [33], who assumed constant gas contribution in fully-closed

cell structures and concluded a best cell size of around 100 μm. However, they also

concluded that the minimum total conductivity corresponds to the minimum radiative

conductivity in fully-closed cell structures [33], in contrast to the results of partially-open cell

structures in Fig. 4-7 and Fig. 4-8.

The total thermal conductivity of the lower solid volume fraction group (Fig. 4-7) is

generally lower than that of the higher solid volume fraction group (Fig. 4-8). This difference

is caused by a change in solid conduction, which accounts for more than 80% of the heat

transfer in the samples (see Fig. 4-7 and Fig. 4-8). The equivalent thermal conductivity of

radiation, which is generally responsible for less than 20% of the total heat transfer, shows a

relatively weak dependence on the solid volume fraction, which is consistent with earlier

observations in Fig. 4-6. Our earlier study [37] of polyurethane foams revealed the similar

proportion of radiative contribution to total heat transfer, namely, 20% of the total heat transfer in vacuum are attributed to radiative transfer.

4-2   The Effects of PE Additive

Figure 4-1, 4-9 and 4-10 show typical SEM pictures of material samples with $0\,wt\%$, $2\,wt\%$ and $5\,wt\%$ PE, respectively. The structure typically consists of struts, cell membranes, broken cells and unbroken cells. Table 4-2 summarizes the measurement results of the samples without PE additive. The samples fall into two distinct groups with different solid volume fraction. The first group, referred to as PE0L, has a lower solid volume fraction, and includes PE0L1 to PE0L6 with $0.0413 < f_s < 0.0494$. The second group, referred to as PE0H, has a higher solid volume fraction and includes PE0H1 to PE0H8 with $0.065 < f_s < 0.0706$. Similar results of samples with $2.0\,wt\%$ and $5.0\,wt\%$ PE additive are also listed in Table 4-2, respectively. Similar to the samples without PE additive in Table 4-2, each PE additive contains two distinct groups with different solid volume fraction. The groups with higher solid volume fraction are designated as PE2H and PE5H, and the groups with lower solid volume fraction are designated as PE2L and PE5L, for the 2% and 5% PE samples, respectively. Note that all solid volume fractions in the 42 investigated samples are extremely low (less than 0.07), indicating a good foaming process. Nevertheless, the distinction between high and low solid volume fractions in each table is sharp and allows us to investigate the effects of solid volume fraction.

Figures 4-11 and 4-12 show examples of spectral transmittance and spectral extinction coefficient, respectively. Note that the spectra do not reveal any CO_2 absorption, which could occur at $2.7\,\mu m$, $4.3\,\mu m$, $9.4\,\mu m$, $10.4\,\mu m$, and $15\,\mu m$, or H_2O absorption, which could occur at $2.7\,\mu m$ and $6.3\,\mu m$. This indicates that the amount of CO_2 and H_2O trapped in the unbroken cells is insignificant in terms of influencing radiation heat transfer. This is reasonable since most of the cells in the samples are broken and evacuated.

4-2-1 The Relationship Description of Physical Properties with PE Additive

Figure 4-13 plots the broken cell ratio versus the cell size. Each group shows an almost linear dependence of cell size on open cell ratio. Higher solid volume fraction is typically associated with larger cell size for a given PE additive weight percentage. The trend can be explained by the fact that a higher solid volume allows the cells to expand further before breaking. In the meantime, in order to obtain a higher broken cell ratio, more of the unbroken cells must be expanded further until they are broken, which also increases the average cell size. Different slopes of the relationship between broken cell ratio and cell size for different PE additive weight percentages in Fig. 4-13 are attributed to the effects of PE on the strength of cell membranes. These effects are also responsible for the larger cell sizes of PE2 and PE5 when compared to PE0. PE0H is an exception because its solid volume fraction is too high, which leads to large cell size as explained earlier. PE's high melting temperature makes them more likely to solidify than PS during the cooling process in foaming and create membrane

45

shear stress when the cells are growing, which helps to raise the broken cell ratio. If the PE additive is too much, however, the cell membrane strength could be augmented too much and the cells would grow larger without becoming broken. It will become evident in the following discussion that 2% PE is appropriate in terms of balancing cell size and broken cell ratio, while 5% PE leads to larger cell size and lower broken cell ratio. To summarize, cell size is influenced by three parameters, the broken cell ratio, the solid volume fraction and the PE additive. Among which, the PE additive is the easiest one to control and is an effective way to modify cell morphology.

4-2-2 The effects of Foam Parameters with PE Additive

Figures 4-15 and 4-16 plot the Rosseland mean extinction coefficient versus the variations in cell size and broken cell ratio, respectively. The extinction coefficient in VIP consists of two parts, the absorption part, σ_α, and the scattering part, σ_s, that is, $\sigma_e = \sigma_\alpha + \sigma_s$. The former represents the absorption effect of solid material and depends largely on the solid volume fraction. The latter is affected by the morphology of the porous foam structure, which is characterized by the average cell size and the broken cell ratio. Smaller cell size implies a shorter mean free path and a larger scattering coefficient for thermal radiation. The mean extinction coefficient therefore increases as the cell size decreases, as evident in Fig. 4-15. For a given PE additive percentage, Fig. 4-16, the group with higher solid volume fraction exhibits only a slight increase in extinction coefficient compared with the lower solid volume

fraction group, although the average solid volume fractions of the two groups differ

significantly. This can be explained by the fact that the solid volume fraction of all the

samples are so small that the extinction is dominated by scattering and the solid absorption

contribution is relatively insignificant. Extinction coefficients generally decrease as the

broken cell ratio increases, as shown in Fig. 4-16, due to reduced scattering by closed cell

membrane. The results in Fig. 4-16 indicate that, although radiation extinction is a complex

process influenced by cell morphology, the broken cell ratio proposed in this study is a

suitable parameter to correlate the extinction coefficient for a given PE additive percentage.

Adding 2% PE is effective in increasing the extinction coefficient, due mainly to the alteration

of cell morphology. Increasing the PE additive to 5% does not increase the extinction further.

On the contrary, the extinction at the same broken cell ratio drops to a lower amount than the

case without PE additive. This can be explained partly by the fact that the cell size has grown

too large in 5% PE samples. The trend in Fig. 4-15 and Fig. 4-16 should be examined

carefully, as the cell size, the solid volume fraction and the broken cell ratio all appear to

influence the extinction coefficient. Nevertheless, the apparent higher extinction coefficient

for higher solid volume fraction shown in Fig. 4-15 can be explained by the lower broken cell

ratio associated with higher solid volume fraction, as evident in Fig.4-13.

4-2-3 The Influences of Lower Solid Fraction without PE Additive

Figure 4-17 shows the equivalent thermal conductivities of samples without PE additive,

including the total thermal conductivity, k_t, the thermal conductivity by solid/gas conduction, k_{s+g}, and the thermal conductivity by radiation, k_r. The total thermal conductivity of the lower solid volume fraction group, PE0L is generally lower than that of the higher solid volume fraction group, PE0H. This difference is mainly caused by a change in solid/gas conduction, which accounts for more than 80% of the heat transfer in the samples. Also, solid/gas conduction increases as the cell sizes decrease, which is associated with lower broken cell ratio and creates more conduction transport routes in the material. On the other hand, radiation decreases as the cell size decreases. Note that the decrease in radiation (increase in extinction coefficient) is attributable to the change in broken cell ratio, as explained earlier. Consequently, there is a best cell size (best broken cell ratio), which leads to the lowest total thermal conductivity after combining k_{s+g} and k_r for each group of samples. In Fig. 4-17, the lowest total thermal conductivity is around 6.5 $mWm^{-1}K^{-1}$, which occurs in the PE0L group at a broken cell ratio of approximately 0.95 corresponding to a cell size of about 100 μm.

4-2-4 The Influences of Higher Solid Fraction with PE Additive

Figure 4-18 and 4-19 shows the equivalent thermal conductivities of PE2 and PE5 groups respectively, with trends similar to that in Fig. 4-16. The best cell size of the 2% PE group, Figure 4-18, falls at around 170 μm, resulting in a total thermal conductivity of 4.4 $mWm^{-1}K^{-1}$, which is the lowest in all the samples investigated in this study. Increasing the

PE additive to 5% does not reduce the total thermal conductivity further. Both solid/gas

conduction and radiation are enhanced in the 5% PE groups when compared to 2% PE group.

The enhanced radiation could be explained by the alteration in cell morphology and the

enhanced solid/gas conduction is explained by the lower broken cell ratios of the 5% PE
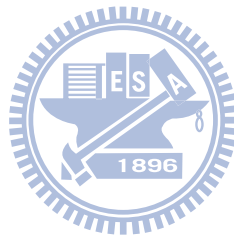
groups, as discussed earlier.

Table 4-1. The experimental results of the 14 samples.

No. of samples	ρ_f	ρ_{f+g}	f_s	ϕ	d_c	σ_e	k_r	k_{s+g}	k_t
	kgm^{-3}	kgm^{-3}			μm	m^{-1}	$mWm^{-1}K^{-1}$	$mWm^{-1}K^{-1}$	$mWm^{-1}K^{-1}$
L1	49	704	0.0494	0.9787	143	5397	1.336	5.46	6.8
L2	47	623	0.0474	0.9705	138	5999.2	1.202	5.50	6.7
L3	44	565	0.0444	0.9649	130	6653.1	1.084	5.52	6.6
L4	43	486	0.0433	0.9528	119	9645.9	0.749	5.75	6.5
L5	42	388	0.0423	0.9312	100	13818.1	0.519	6.48	7.0
L6	41	347	0.0413	0.9198	85	21887.6	0.327	7.37	7.7
H1	70	812	0.0706	0.9832	374	5231.8	1.368	6.73	8.1
H2	69	782	0.0696	0.9799	369	5999.2	1.187	6.71	7.9
H3	68	736	0.0686	0.9744	330	6291.2	1.132	6.67	7.8
H4	65	709	0.0655	0.9720	318	6750.3	1.059	6.64	7.7
H5	64	692	0.0645	0.9701	305	7677.3	0.928	6.67	7.6
H6	63	626	0.0635	0.9604	250	10758.7	0.664	7.24	7.9
H7	62	561	0.0625	0.9488	175	15149.4	0.472	7.83	8.3
H8	61	450	0.0615	0.9211	110	20886.1	0.341	8.66	9.0

Table 4-2. The characteristics of PS core material with 0%PE, 2%PE and 5%PE in vacuum insulation panel.

| No. of samples	ρ_f kgm^{-3}	ρ_{f+g} kgm^{-3}	f_s	ϕ	d_c μm	σ_e m^{-1}	k_r $mWm^{-1}K^{-1}$	k_{s+g} $mWm^{-1}K^{-1}$	k_t $mWm^{-1}K^{-1}$
PE0L1	49	704	0.0494	0.9787	143	5397	1.336	5.46	6.8
PE0L2	47	623	0.0474	0.9705	138	5999.2	1.202	5.50	6.7
PE0L3	44	565	0.0444	0.9649	130	6653.1	1.084	5.52	6.6
PE0L4	43	486	0.0433	0.9528	119	9645.9	0.749	5.75	6.5
PE0L5	42	388	0.0423	0.9312	100	13818.1	0.519	6.48	7.0
PE0L6	41	347	0.0413	0.9198	85	21887.6	0.327	7.37	7.7
PE0H1	70	812	0.0706	0.9832	374	5231.8	1.368	6.73	8.1
PE0H2	69	782	0.0696	0.9799	369	5999.2	1.187	6.71	7.9
PE0H3	68	736	0.0686	0.9744	330	6291.2	1.132	6.67	7.8
PE0H4	65	709	0.0655	0.9720	318	6750.3	1.059	6.64	7.7
PE0H5	64	692	0.0645	0.9701	305	7677.3	0.928	6.67	7.6
PE0H6	63	626	0.0635	0.9604	250	10758.7	0.664	7.24	7.9
PE0H7	62	561	0.0625	0.9488	175	15149.4	0.472	7.83	8.3
PE0H8	61	450	0.0615	0.9211	110	20886.1	0.341	8.66	9.0
PE2L1	30	675	0.0302	0.9854	211	11535.9	0.713	3.89	4.6
PE2L2	29	627	0.0292	0.9825	196	12862.9	0.639	3.86	4.5
PE2L3	28	560	0.0282	0.9776	175	14643.3	0.561	3.84	4.4
PE2L4	26	502	0.0262	0.9737	152	15842.2	0.518	4.48	5.0
PE2L5	25	448	0.0252	0.9686	140	17153.1	0.479	4.82	5.3
PE2H1	52	761	0.0524	0.9832	252	12825.8	0.640	4.66	5.3
PE2H2	51	732	0.0514	0.9808	238	13729.1	0.598	4.60	5.2
PE2H3	49	695	0.0494	0.9778	212	14920.2	0.552	4.55	5.1
PE2H4	48	668	0.0484	0.9753	191	15482.9	0.531	5.07	5.6
PE2H5	47	637	0.0474	0.9723	177	16655.2	0.495	5.31	5.8
PE5L1	49	762	0.0494	0.9843	264	5488.4	1.497	5.90	7.4
PE5L2	49	695	0.0492	0.9778	263	5545.8	1.484	5.72	7.2
PE5L3	48	579	0.0476	0.9637	262	6081.8	1.352	5.85	7.2
PE5L4	47	540	0.0465	0.9584	245	6959.4	1.181	5.92	7.1
PE5L5	46	473	0.0464	0.9466	240	8643.4	0.953	6.05	7
PE5L6	46	452	0.0454	0.9419	239	8664.4	0.949	6.05	7
PE5L7	46	382	0.0451	0.9224	220	9669.6	0.849	5.95	6.8
PE5L8	45	334	0.0444	0.9064	180	15161.5	0.540	6.56	7.1
PE5L9	44	319	0.0436	0.9021	145	16771.1	0.488	7.11	7.6
PE5H1	65	706	0.0655	0.9716	302	6420	1.279	6.62	7.9
PE5H2	64	655	0.0649	0.9645	296	6750.7	1.214	6.49	7.7
PE5H3	64	523	0.0647	0.9592	276	6891.5	1.189	6.51	7.7
PE5H4	63	509	0.0638	0.9357	251	9658.9	0.850	6.45	7.3
PE5H5	63	476	0.0635	0.9265	226	11612.5	0.707	6.49	7.2
PE5H6	62	460	0.0626	0.9229	241	12452.4	0.658	6.44	7.1
PE5H7	61	440	0.0617	0.9178	217	13162.3	0.624	6.68	7.3
PE5H8	61	431	0.0616	0.9147	197	14666.1	0.599	6.9	7.5
PE5H9	60	393	0.0604	0.9019	140	18567.8	0.441	7.56	8.0
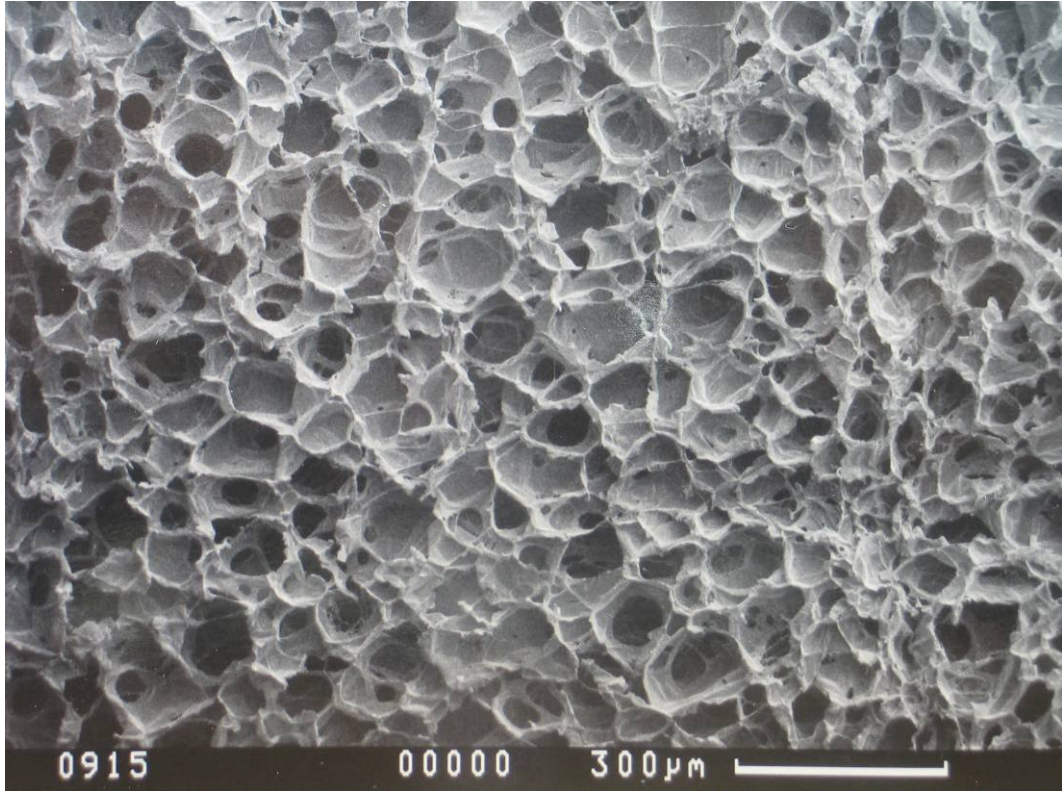
Figure 4-1. The SEM picture of sample L4.
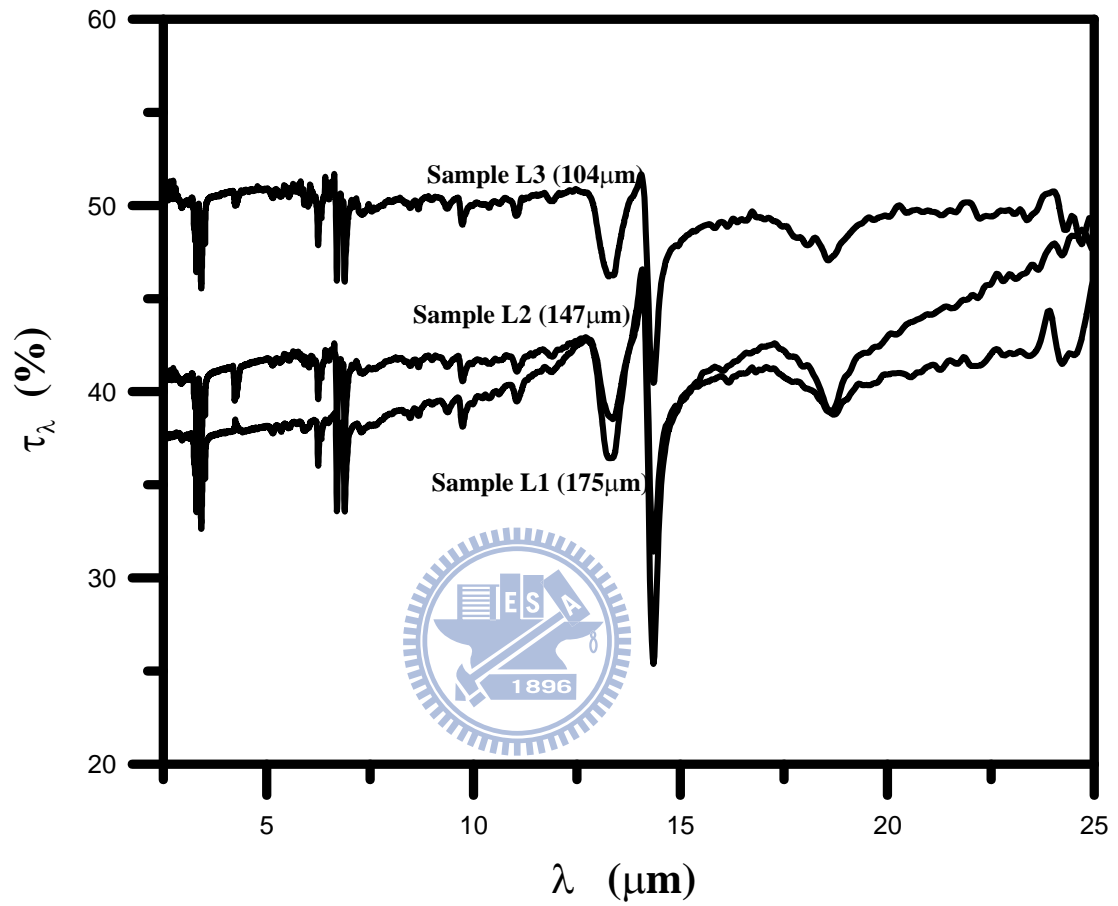
Figure 4-2. The transmittance spectrums of several typical samples.
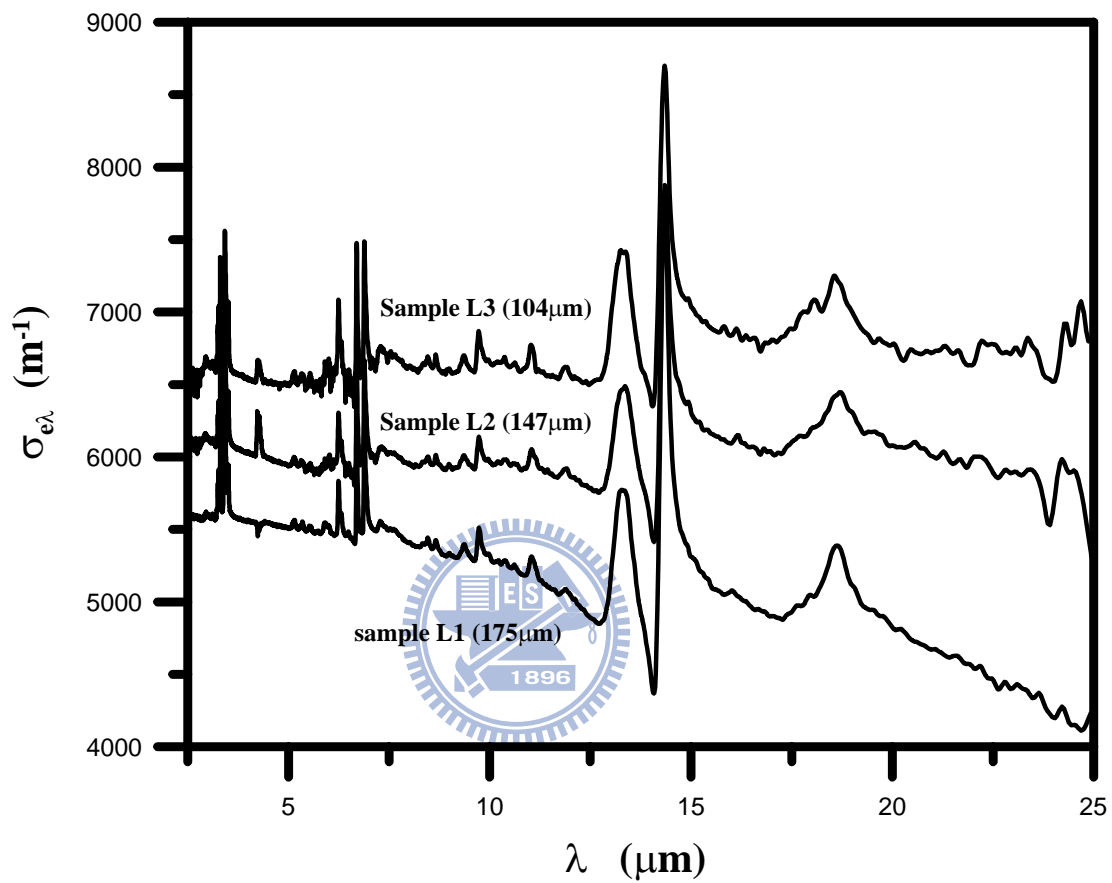
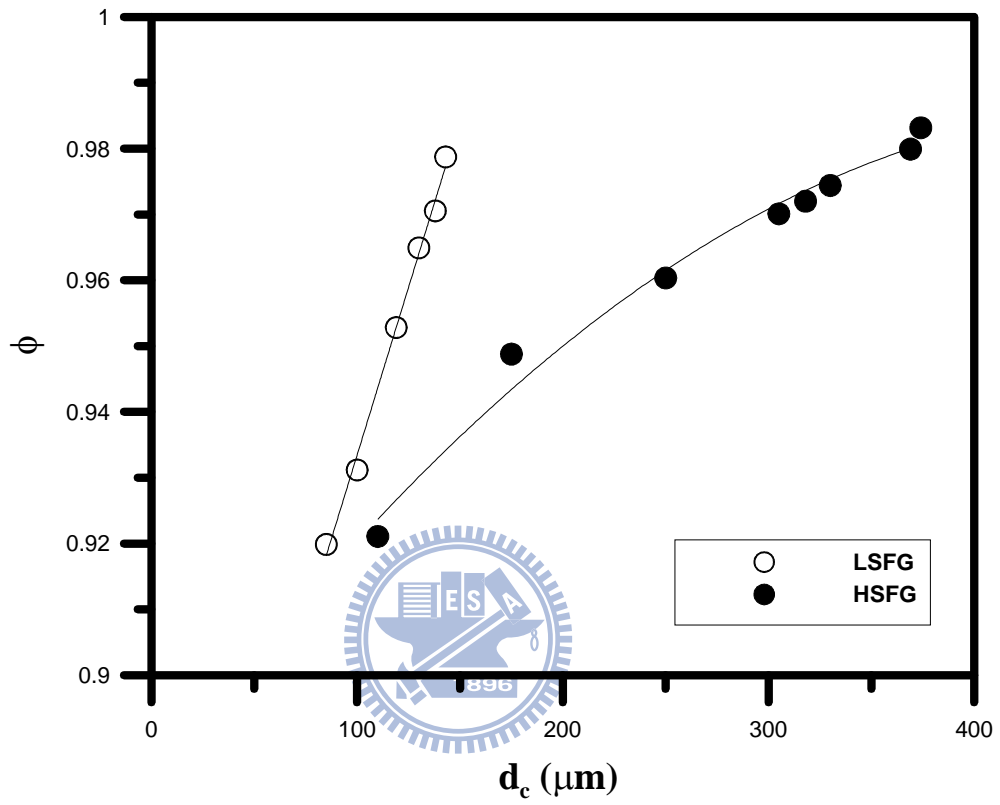Figure 4-3. The spectral extinction coefficients of several typical samples.

Figure 4-4. The relation between average cell size and broken cell ratio, under two different solid volume fractions.
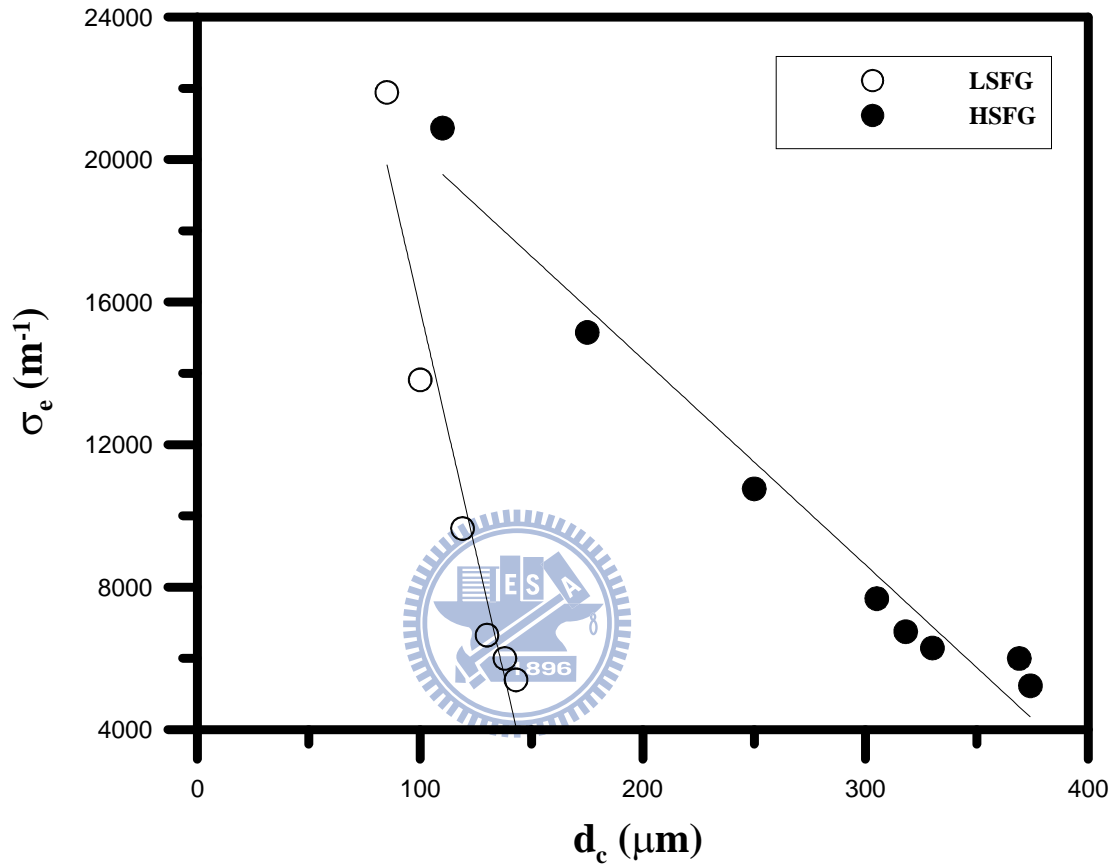
Figure 4-5. The effects of average cell size on extinction coefficient, under two different solid volume fractions.
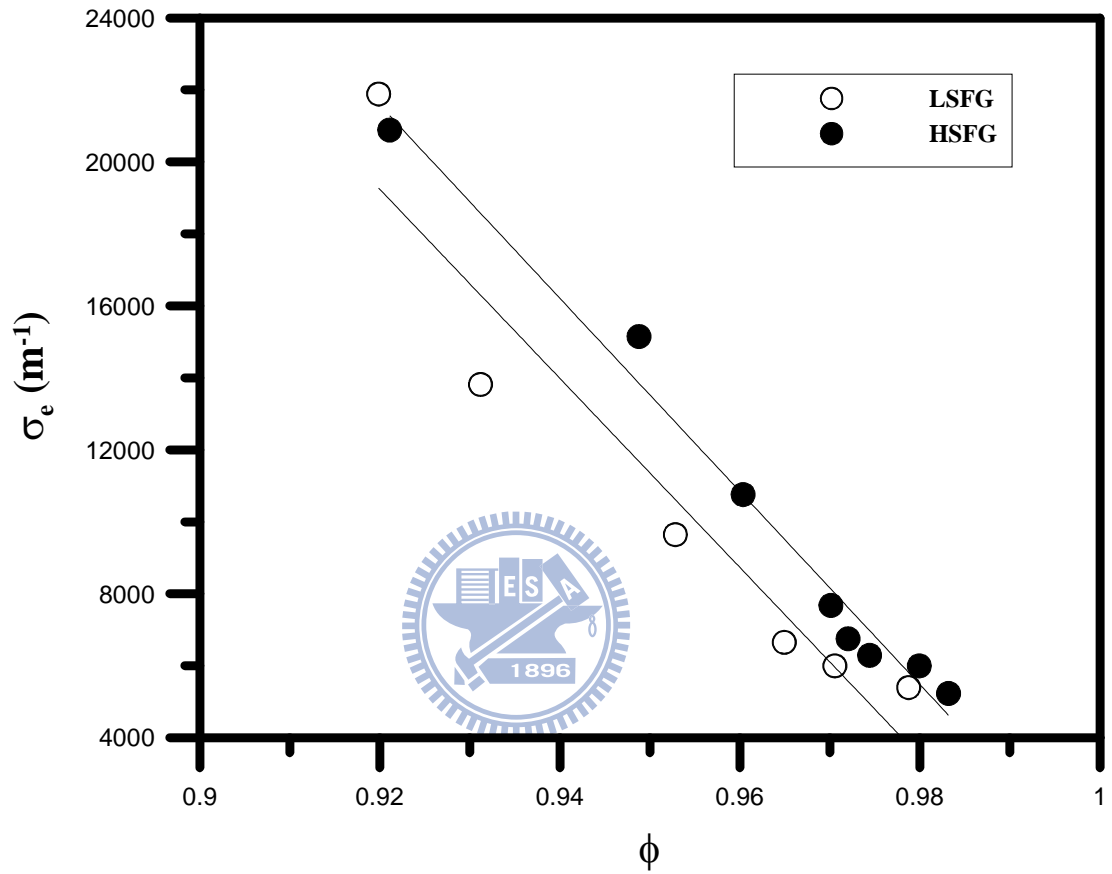
Figure 4-6. The effects of broken cell ratio on extinction coefficient, under two different solid volume fractions.
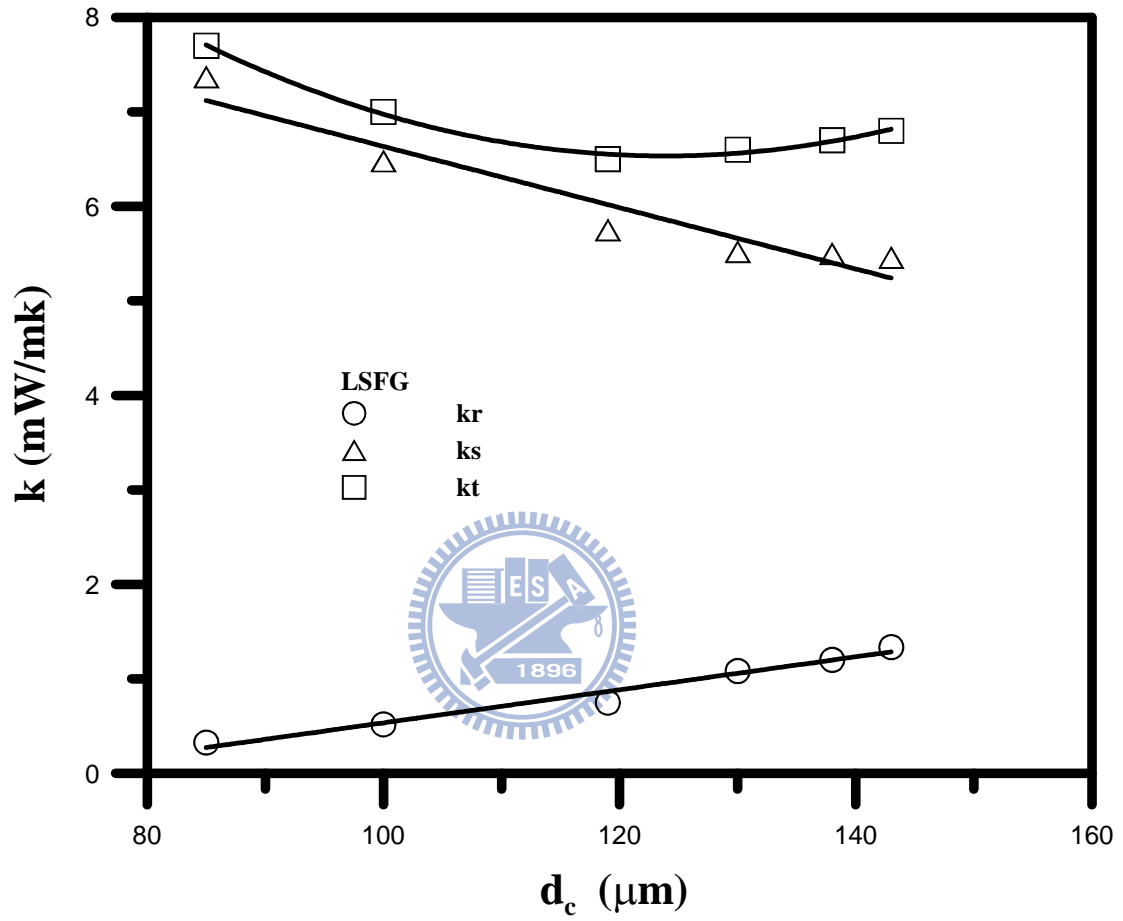
Figure 4-7. The influences of average cell size on the LSFG equivalent thermal conductivities.
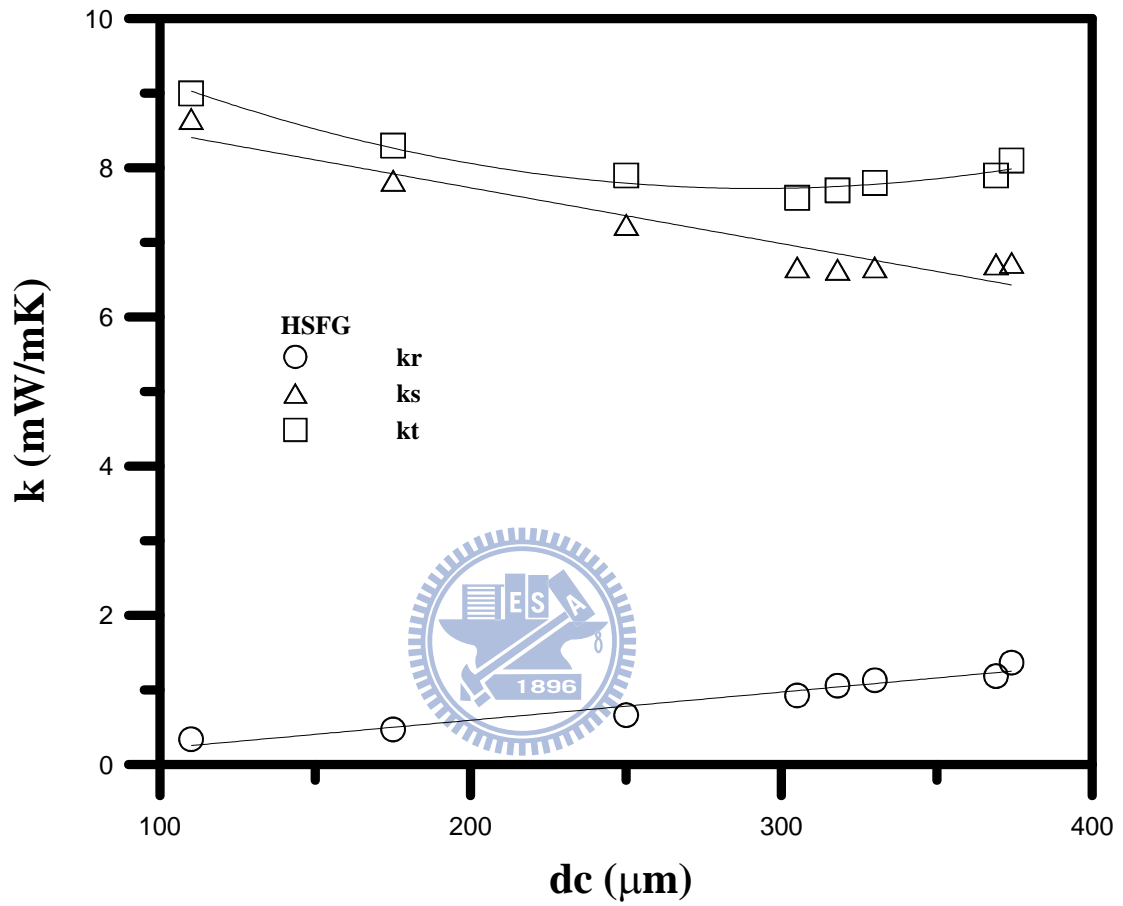
Figure 4-8. The influences of average cell size on the HSFG equivalent thermal
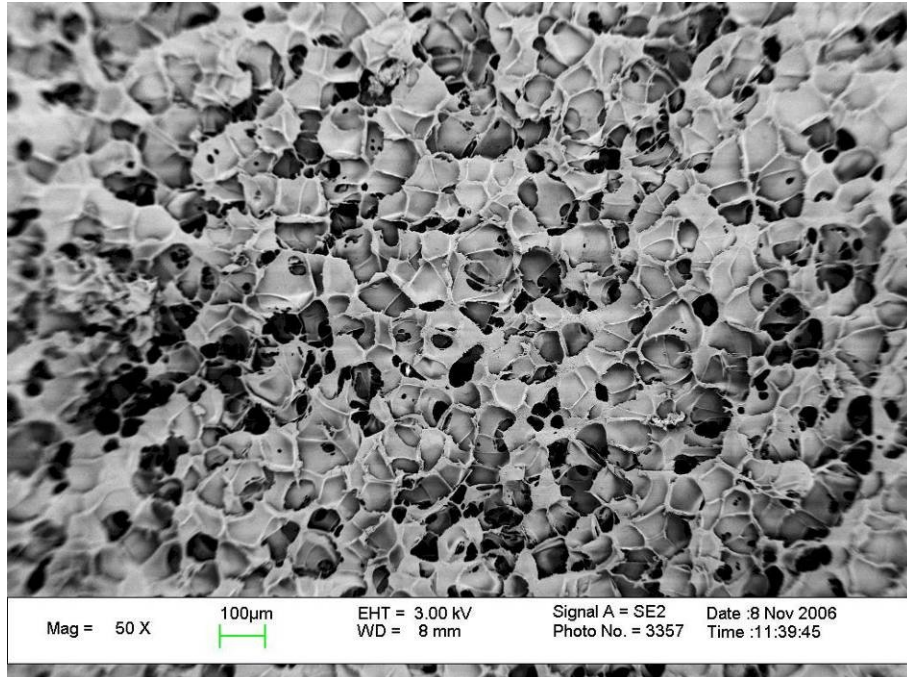conductivities.

Figure 4-9. SEM of sample PE2L1 for PS core material with 2% PE additive.
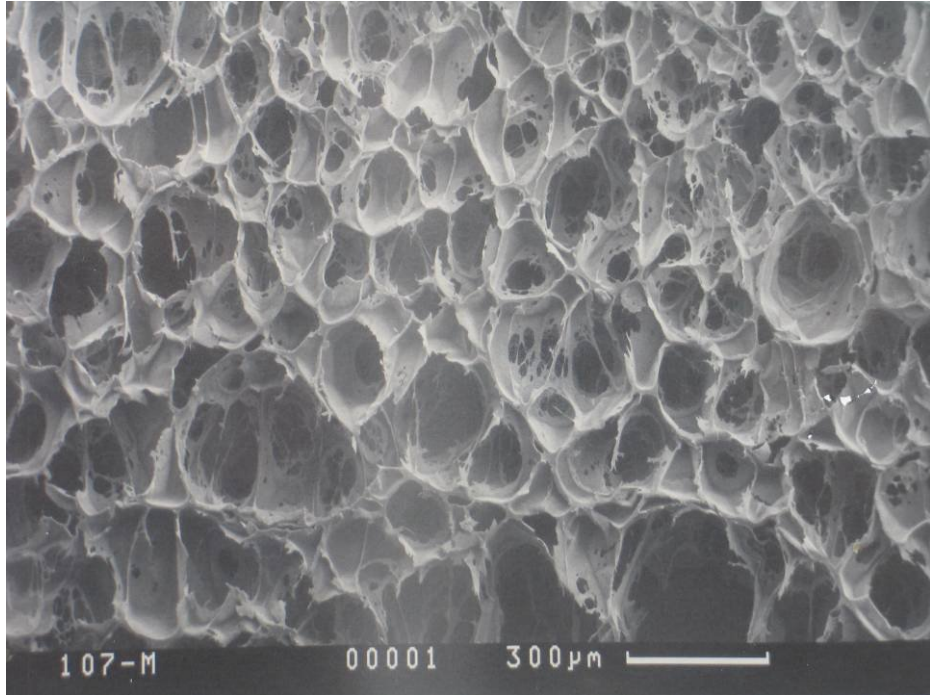
Figure 4-10. SEM of sample PE5L3 for PS core material with 5% PE additive.
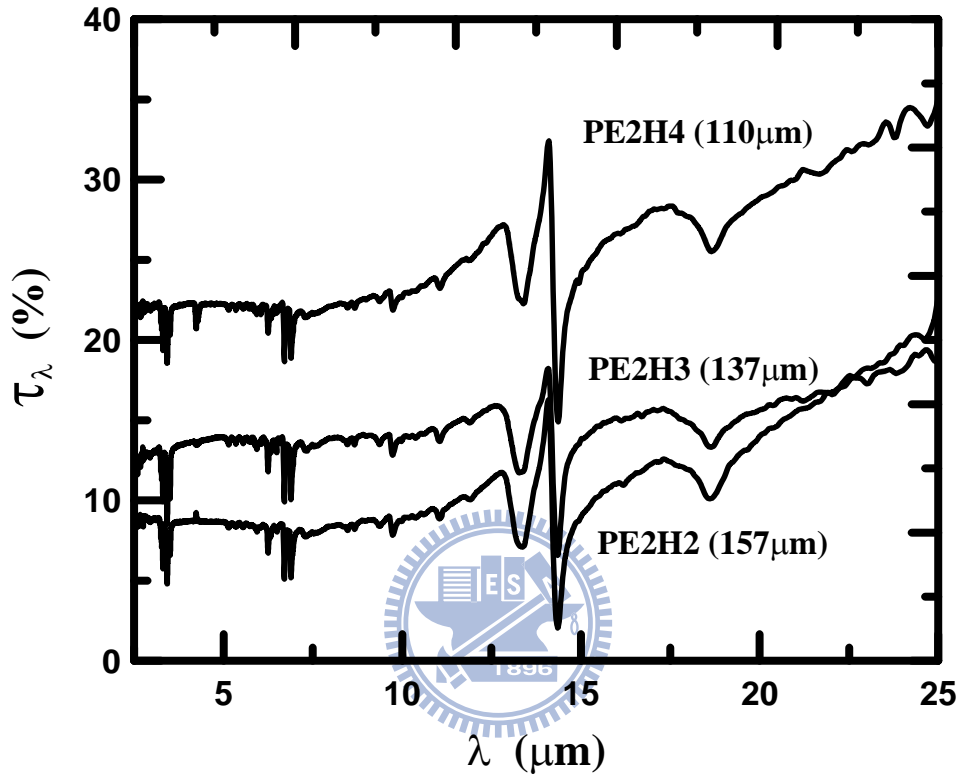
Figure 4-11. Spectral transmittance varied with wavelength on PE2H samples
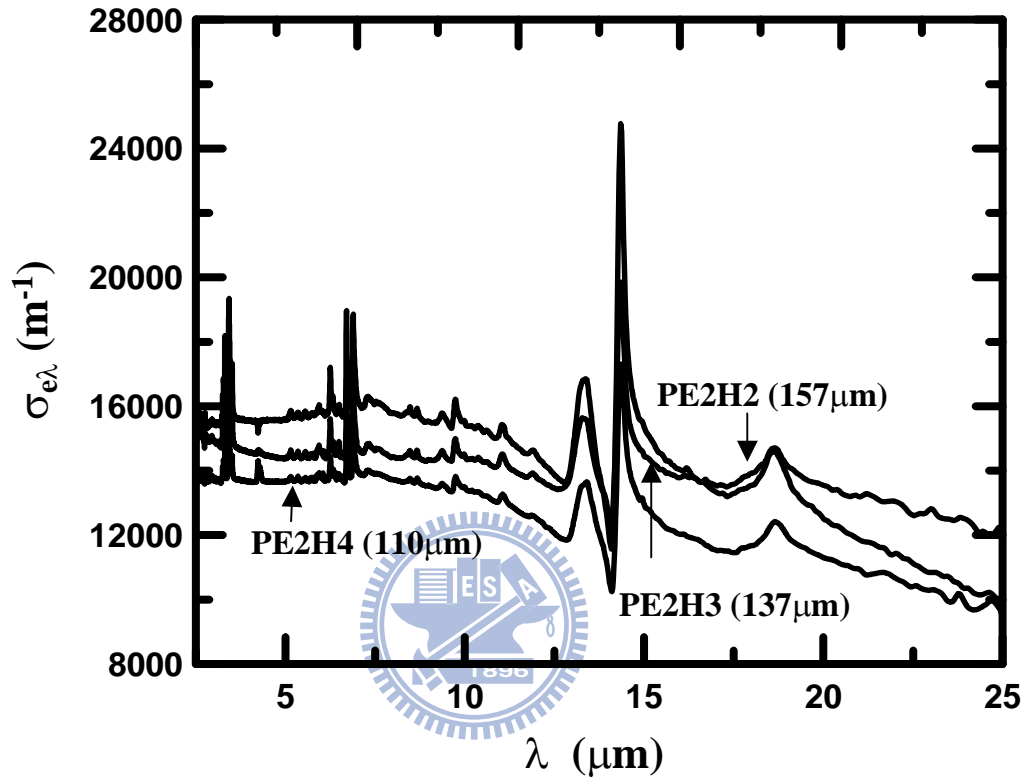
Figure 4-12. Spectral extinction coefficient varied with wavelength on PE2H samples.
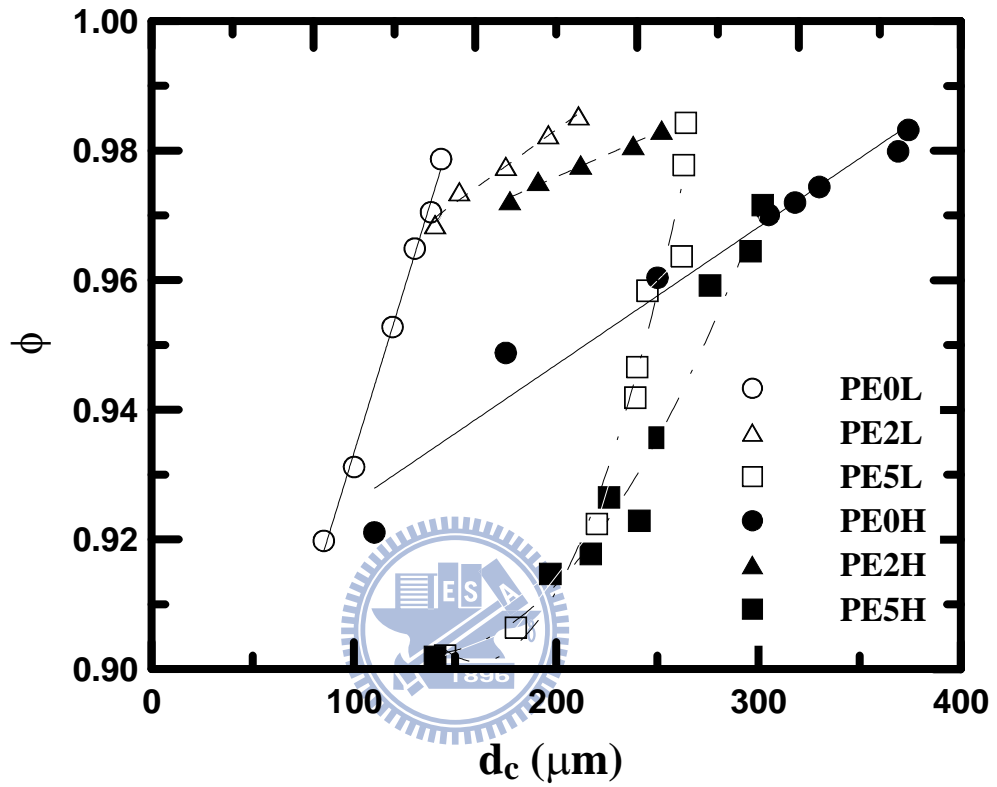
Figure 4-13. Relationship between cell sizes and broken cell ratio on various PE additives with high and low solid volume fraction.
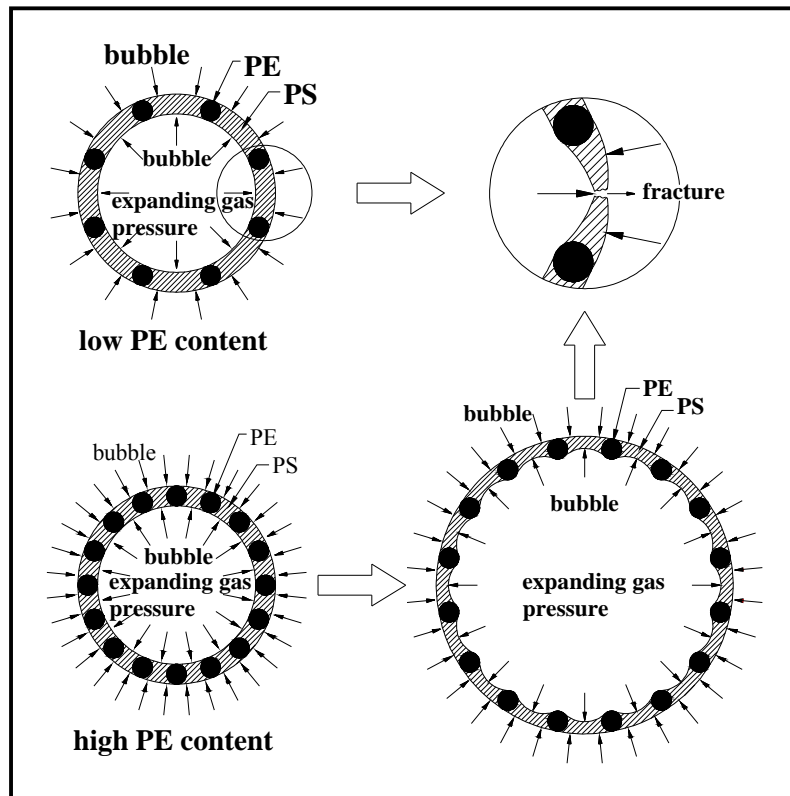
Figure 4-14. The mechanisms of PE additive acting on cell membrane broken
in the growing cell.
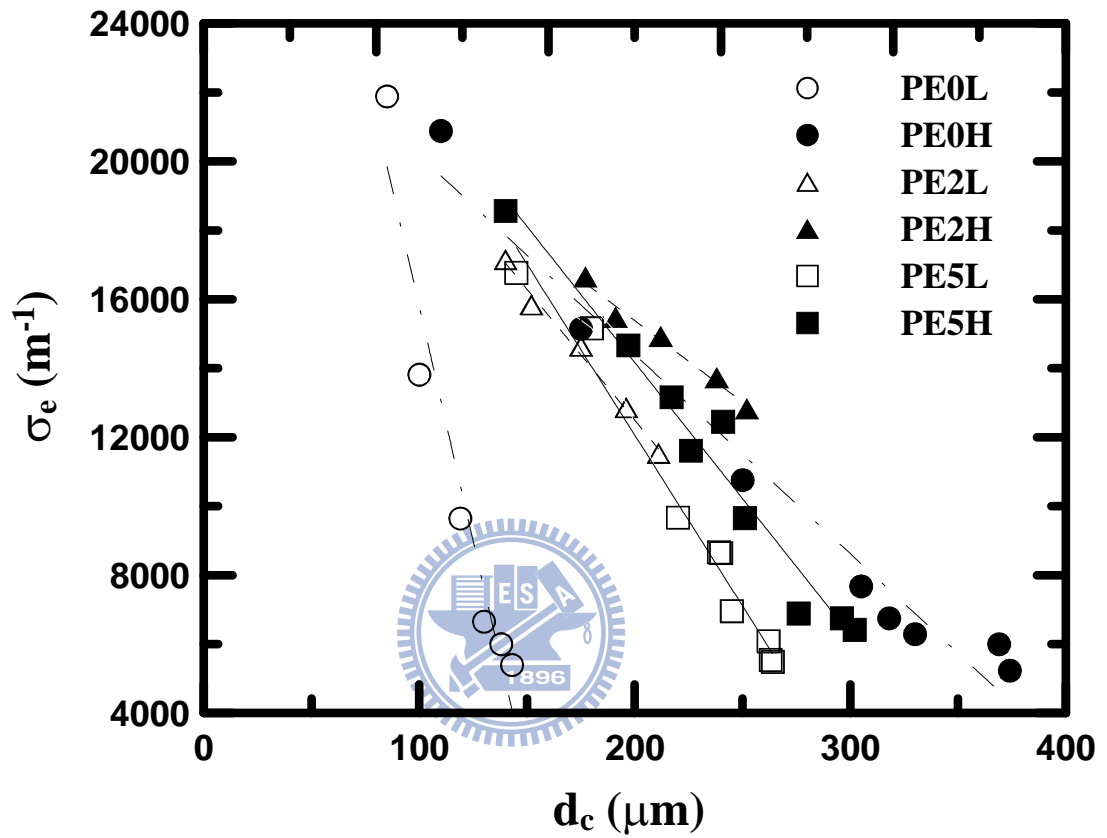
Figure 4-15. Rosseland mean extinction coefficient varied with cell sizes with/without
PE additives on high and low solid volume fraction.
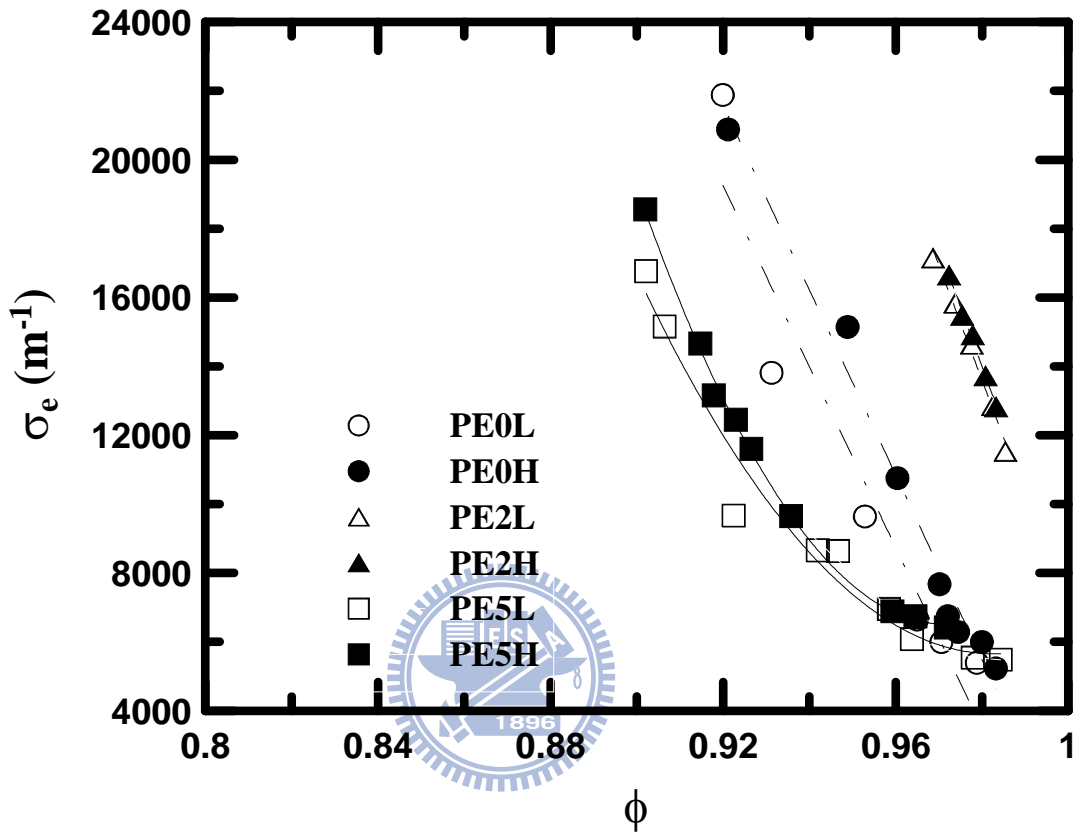
Figure 4-16.Rosseland mean extinction coefficient varied with broken cell ratio
with/without PE additives on high and low solid volume fraction.
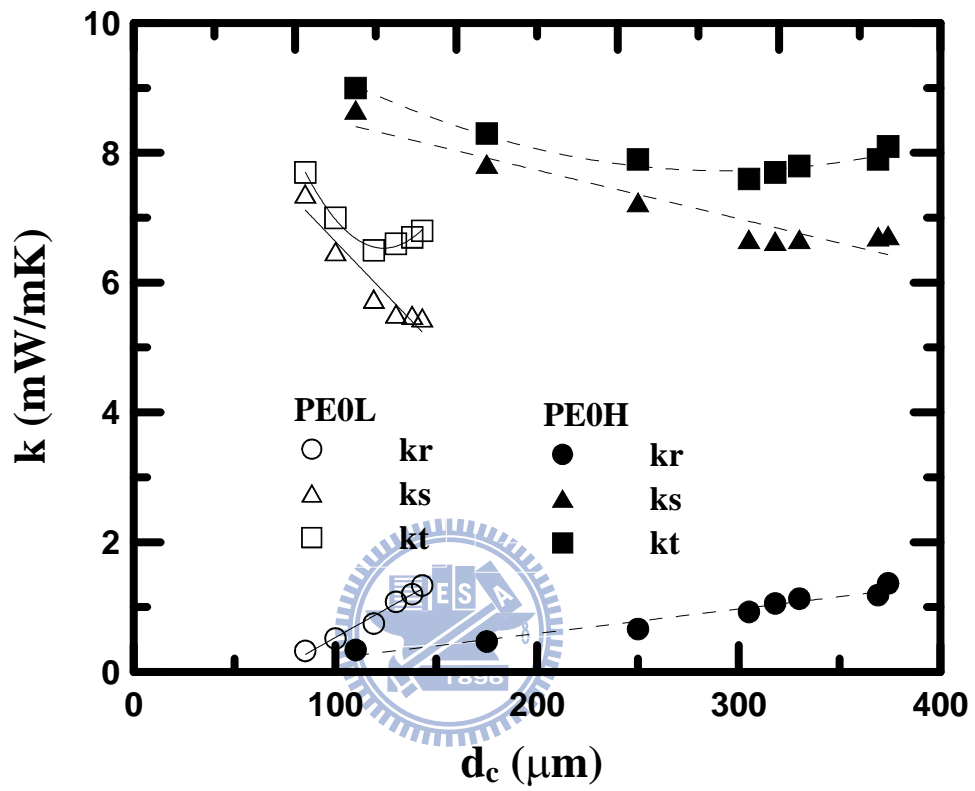
Figure 4-17. The relation between equivalent thermal conductivity and cell sizes for PS core material without PE additive.
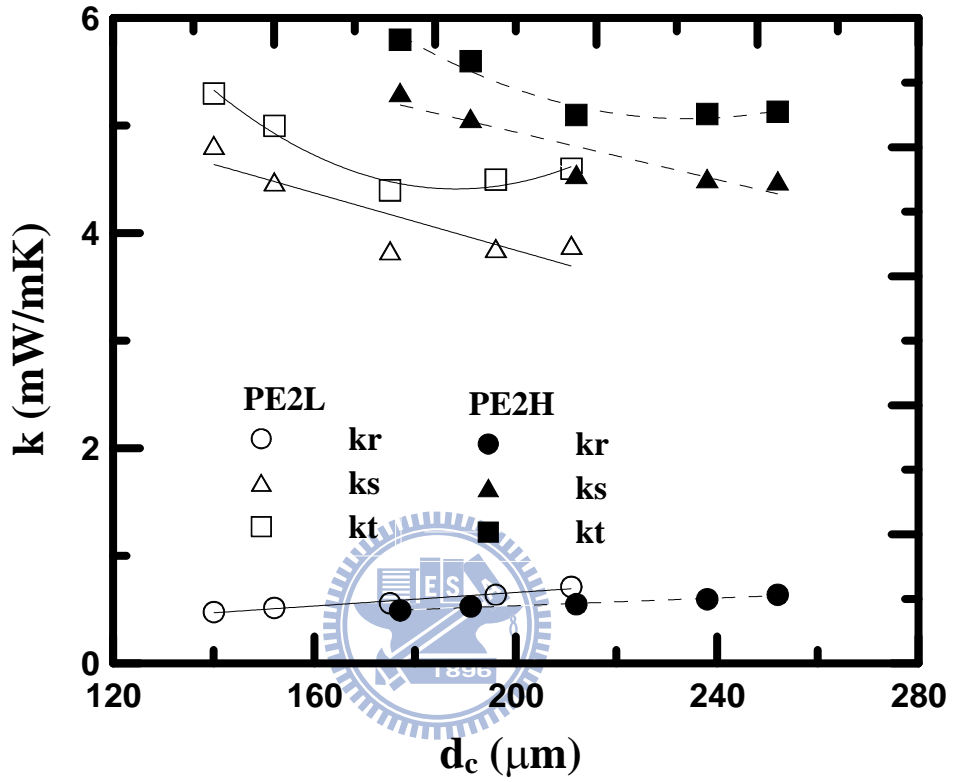
Figure 4-18. The relation between equivalent thermal conductivity and cell sizes for PS core material with 2% PE additive.
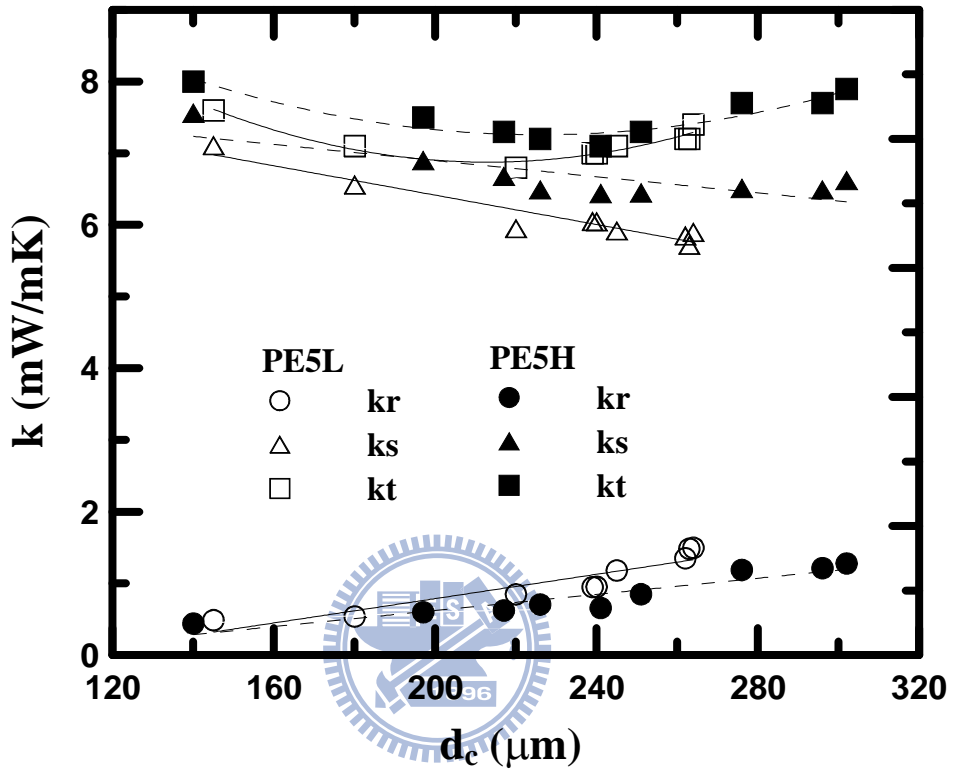
Figure 4-19. The relation between equivalent thermal conductivity and cell sizes for
PS core material with 5% PE additive.

CHAPTER 5

CONCLUSIONS AND RECOMMENDATIONS

5-1 Conclusions

This study analyzes heat transfer in practical VIPs, that is, VIPs with a broken cell ratio higher than 90%. The structure of these non-black-body VIP foams consists of struts, closed cells, and open cell residue membranes. Two parameters, namely, the broken cell ratio and the average cell size, are proposed to characterize the cell structure. The experimental samples are further grouped based on their solid volume fraction to reveal the influence of the solid material on heat transfer. Some conclusions derived from the experimental findings are summarized below.

1. Radiation heat transfer, as manifested by the mean extinction coefficient, is influenced predominantly by the broken cell ratio. The effects of cell size and solid volume fraction upon radiation are relatively insignificant in the samples investigated in this study.

2. Under a specific solid volume fraction, the best broken cell ratio (best cell size) leads to the lowest total thermal conductivity.

3. Solid volume could affect the absorption coefficient in radiation transfer, but the effects are not obvious because the solid volume fraction is extremely low in this study, and the extinction coefficient is dominated by scattering. However, the solid volume fraction has a crucial effect on solid conduction, which is the dominant heat transfer mechanism in VIP.

A rule of thumb to improve VIP performance can be derived from the findings in this study. Firstly, the solid volume fraction must be kept low to diminish the solid conduction. Secondly, the cell size and broken cell ratio must be carefully controlled to an optimum value to produce the lowest total thermal conductivity. A high broken cell ratio may cause high radiation transfer, and does not necessarily imply low total thermal conductivity. Experimental results of this study suggest a best cell size in the range of 100 to 300 μm for practical VIP with a high broken cell ratio.

The structure of these non-black-body VIP foams consists of struts, closed cells and open cell residue membranes. PE additive is used as a way to alter the foam structure and the heat transfer. Two parameters, namely, the broken cell ratio and the average cell size, are proposed to characterize the structure. The experimental samples are further grouped based on their solid volume fraction to reveal the influence of the solid material on heat transfer. Some conclusions derived from the experimental findings may help improve VIP performance, as summarized below.

4. Under a specific solid volume fraction, a best cell size (best broken cell ratio) leads to the lowest total thermal conductivity.

5. Radiation heat transfer, as manifested by the mean extinction coefficient, is influenced predominantly by broken cell ratio. The effects of solid volume fraction upon radiation are relatively insignificant in the samples investigated in this study. PE2 samples have smaller

cell size and therefore higher extinction than PE5 samples.

6. An appropriate amount of PE additive has proven to be effective in tuning the cell structure and improving the VIP performance. The best PE additive percentage found in this study was 2%.

7. Solid volume could affect the absorption coefficient in radiation transfer, but the effects are not obvious because the solid volume fraction is extremely low in this study, and the extinction coefficient is dominated by scattering. However, the solid volume fraction has a crucial effect on solid conduction, which is the dominant heat transfer mechanism in VIP. A rule of thumb to improve VIP permeance can be derived from the findings in this study. Firstly, the solid volume fraction must be kept low to diminish the solid conduction. Secondly, the cell size and broken cell ratio must be carefully controlled to an optimum value to produce the lowest total thermal conductivity. A high broken cell ratio may cause high radiation transfer, and does not necessarily imply low total thermal conductivity. In contrast to conventional closed-cell foam, where a small cell size reduces the heat transfer of trapped gas, the best cell size in practical VIP with high broken cell ratio ranges from 100 to 300 μm. The lowest thermal conductivity obtained in this study reached $4.4\,mWm^{-1}K^{-1}$, and was among the best when previously compared to published VIP performance results.

5-2 Recommendations

In the future, a key factor in further reducing the thermal conductivity of VIP is the elimination of solid conduction, which accounts for 90% of VIP's total heat transport according to the results of this study. One attractive approach is to reduce the mass or volume of the solid material as much as possible, thus diminishing the solid conduction readily. Nevertheless, the extremely low solid content poses new challenges not only to manufacturing but also to maintaining low thermal radiation. The cell membranes are generally thin due to the low solid content and become more transparent to thermal radiation. The low solid content also implies weak structural support from the solid material, such that the cell size must be reduced to maintain structural integrity. Small struts and nodes associated with the small cell size may no longer be effective in scattering thermal radiation, thus the radiative heat transport is increased. By largely reducing solid content and balancing solid conduction and thermal radiation, one should be able to attain extremely low thermal conductivity at an optimal solid content, which was not pursued in this study mainly due to the manufacturability limitation inherent in the in-house facility employed in this study.

REFERENCES

1. C.L. Tien and G.R. C.R. Cunnington, Cryogenic insulation heat transfer, Advances in Heat Transfer 9(1973)349-417.

2. L.J. Gibson and M.F. Ashby, Cellular solids-structure and properties, Cambridge university, 1997.

3. N.C. Hilyard and A. Cunningham, Low density cellular plastic-physical basis of behaviour, Champan & Hall,London, 1994.

4. B. Griffith and D. Arasteh, Advanced insulations for refrigerator/freezers: the potential for new shell designs incorporating polymer barrier construction, Energy and Buildings 22(3)(1995)219-231.

5. H.W. Fraser and J.C. Jofriet, Thermal behaviour of polyurethane foam insulation, Canadian Agricultural Engineering 35(1)(1993)57-65.

6. C.J. Tseng, M. Yamaguchi and T. Ohmori, Thermal conductivity of polyurethane foams from room temperature to 20 K, Cryogenics 37(6)(1997)305-312.

7. H.S. Chu and C.J. Tseng, Analysis of Radiative Heat Transfer in Ultra-Fine Powder Insulations Under Variation of Radiative Boundary Conditions, Journal of Building Physics 12(2)(1988)108-123.

8. J.Kuhn, H.P. Ebert, M.C. Arduini-Schuster, D. BUTTNER and J.Fricke, Thermal transport in polystyrene and polyurethane foam insulations, Int. J. Heat Mass Transfer 35(7) (1992)

1795-1801.

9. Gerard Marie Rene du CAUZE de NAZELLE, Thermal conductivity ageing of rigid closed cell polyurethane foams, The Hague, The Netherlands, 1995.

10. K.W. Suh et al., US Patent No. 5679718, 1997.

11. D.D. Imeokparia et al., US Patent No. 5693687, 1997.

12. C.D. Shmidt et al., US Patent No. 5780521, 1998.

13. Bruce A. Malone, US Patent No. 5844014, 1998.

14. K.W. Suh et al., US Patent No. 5854295, 1998.

15. B. A. Malone, US Patent No. 5858501, 1999.

16. B. A. Malone, US Patent No. 5977197, 1999.

17. J. Fricke, U. Heinemann, and H.P. Ebert, Vacuum insulation panels-From research to market, Vacuum 82(2008)680-690.

18. T.W. Tong and C.L. Tien, Radiative heat transfer in fibrous insulations-part I: analytical study, Transactions of the ASME 105(1983)70-75.

19. T.W. Tong, Q.S. Yang and C.L. Tien, Radiative heat transfer in fibrous insulations-part II: analytical study, Transactions of the ASME 105(1983)76-81.

20. T.W. Tong and C.L. Tien, Analytical models for thermal radiation in fibrous insulations, Journal of Thermal Insulation 4(1980)27-43.

21. H.S. Chu, A.J. Stretton and C.L. Tien, Radiative heat transfer in ultra-fine

powder insulations, Int. J. Heat Mass Transfer 31(8) (1988) 1627-1634.

22. A. L. Marge, The use of coated micropowders to reduce radiation heat transfer in foam insulation, Massachusetts Institute of Technology, June 1991.

23. U. Heinemann and R. Caps, Radiation-conduction interaction: an investigation on silica Aerogels, Int. J. of Heat Mass Transfer 39(10)(1996) 2115-2130.

24. M.A. Schuetz, Heat transfer in foam insulation, Massachusetts Institute of Technology, September 1982.

25. M.A. Schuetz and L.R. Glicksman, A basic study of heat transfer through foam insulation, Journal of Cellular Plastics (1984)114-121.

26. M.R. Toroey, A study of radiative heat transfer through foam insulation, Massachusetts Institute of Technology, September 1987.

27. A.M. Druma, M.K. Alam and C. Druma, Analysis of thermal conduction in carbon foams, Int. J. Thermal Sciences 43 (2004) 689-695.

28. R.Caps, U. Heinemann, J. Fricke and K.Keller, Thermal conductivity of polymide foams, Int. J. Heat Mass Transfer 40(2) (1997) 269-280.

29. L.R. Glicksman and M. R. Torpey, The influence of cell size and foam density on the thermal conductivity of foam insulation, Polyurethanes World congress (1987) 80-84, Aachen, Germany, Sept.29-Oct. 2.

30. M. D. Mozgowiec, The use of small cells to reduce radiation heat transfer in foam

insulation, Massachusetts Institute of Technology, June 1990.

31. M.C. Page, Effects of alternate blowing agents on the aging of closed-cell foam insulation, Massachusetts Institute of Technology, June 1991.

32. L.R. Glicksman, A. L. Marge and J. D. Moreno, Radiation heat transfer in cellular foam insulation, ASME Paper HTD-203 (1992) 45-53, Developments in Radiative Heat Transfer.

33. E.Placido, M.C. Arduini-Schuster and J. Kuhn, Thermal properties predictive model for insulating foams, Infrared Physics & Technology 46 (2005) 219-231.

34. B.K. Larkin and S.W. Churchill, Heat transfer by radiation through porous insulations, A.I.Ch.E. Journal 5(4)(1959)467-474.

35. M. Arduini and F. de Ponte, Combined radiation and conduction heat transfer in insulating materials, High Temperature-High Pressures, 19(1987)237-249.

36. V. Giaretto, E. Miraldi and G. Ruscica, Simultaneous estimations of radiative and conductive properties in lightweight insulating materials, High Temperature – High Pressures 27/28 (1995/1996) 191-204.

37. J.W. Wu, W.F. Sung and H.S. Chu, Thermal conductivity of polyurethane foams, Int. J. Heat Mass Transfer 42 (1999) 2211-2217.

38. H.Y. Li, Estimation of thermal properties in combined conduction and radiation, Int. J. Heat Mass Transfer 42(1999)565-572.

39. D.Doermann and J.F. Sacadura, Heat transfer in open cell foam insulation, ASME J. Heat Transfer 118 (1996) 88-93.

40. K. Kamiuto, Study of Dul'nev's model for the thermal and radiative properties of open-cellular porous materials, JSME Int. J. Series B 40(4) (1997) 577-582.

41. D. Quenard and D. Giraud, Heat transfer in the packing of cellular pellets: microstructure and apparent thermal conductivity, High Temperatures-High Pressures 30(6) (1998) 709-715.

42. D. Baillis, M. Raynaud and J. F. Sacadura, Spectral radiative properties of open-cell foam insulation, Journal of Thermophysics and Heat Transfer 13(3)(1999)292-298.

43. T.J. Lu, H.A. Stone, and M.F. Ashby, Heat transfer in open-cell metal foams, Acta mater 46(10)(1998)3619-3635.

44. C.Y. Zhao, T.J. Lu and H.P. Hodson, Thermal radiation in ultralight metal foams with open cells, Int. J. Heat Mass Transfer 47(2004) 2927-2939.

45. C.Y. Zhao, T.J. Lu, H.P. Hodson, The temperature dependence of effective thermal conductivity of open-celled steel alloy foams, Material Science and Engineering (2004) A 367 123-131.

46. C. De Micco and C. M. Aldao, Radiation contribution to the thermal conductivity of plastic foams, J. Polym. SCI. Part B: Poly: 43 (2005) 190-192.

47. M. Wang and N. Pan, Modeling and prediction of the effective thermal conductivity of

random open-cell porous foams, Int. J. Heat Mass Transfer 51(5-6)(2008)1325-1331.

48. C.H. Ho and M.N. Özisik, Simultaneous conduction and radiation in a two-layer planar medium, Journal of Thermophysics and Heat Transfer1(2)(1987)154-161.

49. B. Zeghondy, E. Iacona, J. Taine, Determination of the anisotropic radiative properties of a porous material by radiative distribution function identification (RDFI), Int. J. Heat Mass Transfer 49 (2006) 2810-2819.

50. B. Zeghondy, E. Iacona, J. Taine, Experimental and RDFI calculated radiative properties of a mullite foam, Int. J. Heat Mass Transfer 49 (2006) 3702-3707.

51. M. Tancrez, J. Taine, Direct identification of absorption and scattering coefficients and phase function of a porous medium by a Monte Carlo technique, Int. J. Heat and Mass Transfer 47 (2004) 373-383.

52. M. Loretz, R. Coquard, D. Baillis, and E. Maire, Metallic foams: Radiative properties/comparison between different modes, J. Quantitative Spectroscopy & Radiative Transfer 109 (2008) 16-27.

53. R. Coquard and D. Baillis, Modeling of heat transfer in low-density EPS Foams, ASME J. Heat Transfer 128 (June 2006) 538-549.

54. T.H. Bauer, A general analytical approach toward the thermal conductivity of porous media, Int. J. Heat Mass Transfer 36(17)(1993)4181-4191.

55. O.A, Almanza, M.A. Rodriguez-Perez, and J.A. De Saja, Prediction of the radiation term

in the thermal conductivity of crosslinked closed cell polyolefin foams, Journal of polymer Science: Part B: Polymer Physics, 38(2000)993-1004.

56. C.J. Tseng and K.T. Kuo, Thermal radiative properties of phenolic foam insulation, Journal of Quantitative Spectroscopy & Radiative Transfer 72(2002)349-359.

57. D.Baillis, M. Arduini-Schuster and J.F. Sacadura, Identification of spectral radiative properties of polyurethane foam from hemispherical and bi-directional transmittance and reflectance measurements, J. Quantitative Spectroscopy & Radiative Transfer 73 (2002) 297-306.

58. M.N. Özisik, Radiative transfer and interactions with conduction and convection, John Wiley & Sons, New York, 1973.

59. R. Siegel, and J.R. Howell, Thermal radiation heat transfer, 4th Ed., Taylor & Francis, New Yoke, London, 2002.

60. R.R. Zarr and E.S. Lagergren, Development of thermal insulation standard reference materials using good experimental design, Thermal Conductivity, 24th and Thermal Expansion. 12th Joint Conferences Proceedings, October 26-29,1997.

LIST OF PUBLICATION

1. P.C. Tseng, and H.S. Chu, An experimental study of the heat transfer in PS foam insulation, Heat Mass Transfer (2009) 45:399-406.

2. P.C. Tseng, and H.S. Chu, The effect of PE additive on the performance of polystyrene vacuum insulation panels, Int. J. Heat and Mass Transfer 52(2009)3084-3090.